

# Conductance of Mesoscopic Rings

by

Rangga P. Budoyo

Class of 2008

A thesis submitted to the  
faculty of Wesleyan University  
in partial fulfillment of the requirements for the  
Degree of Bachelor of Arts  
with Departmental Honors in Physics

# Abstract

In the studies of conductance of closed mesoscopic systems, semi-linear response theory (SLRT) offers a novel unified framework that goes beyond the traditional Kubo formulation. In this Thesis we apply SLRT to two types of mesoscopic systems. The first is disordered quasi-1d rings, where we build an analytical model to understand the departure of SLRT results from Kubo results. Guided by the numerical analysis on the statistical properties of the current operator matrix elements, we introduce a random matrix theory (RMT) model which leads to a generalized variable range hopping (VRH) picture of the conductance. Both of these models capture the essential aspects of the mesoscopic conductance for this system. The second system is the Harper model, which is a one-dimensional model that exhibits a Metal-Insulator transition—at the critical point, it possesses fractal structures in both the eigenfunctions and the eigenvalues. We are interested in studying how the fractal structures might have an effect on the mesoscopic conductance calculations.

# Acknowledgments

Writing this Thesis has been challenging and difficult, but overall it is a very inspiring and satisfying experience. Here, I would thank the people that give contribution in some way or another to the completion of this Thesis.

First and foremost, I am very grateful to have Tsampikos Kottos as my advisor, as he offered almost constant help, advice, and support for this past year and a half. I would like to acknowledge Doron Cohen, Alexander Stotland, Jiayi Zhang, and Tal Peer for the insightful collaborations. I would also like to thank Gim Seng Ng, Joshua Bodyfelt, Moritz Hiller, and the rest of the Wesleyan CQDMP Group members for the helpful discussions. I would like to thank Joshua again for helping with the correction of this Thesis.

Wesleyan University is gratefully acknowledged for the financial support. Financial support from the USA-Israel Binational Science Foundation (BSF) and the DFG Forschergruppe 760 are also acknowledged.

I would also like to thank all the professors at Wesleyan University for their help and guidance during my almost four years of study here and the people in the MPI for Dynamics and Self-Organization Göttingen for their hospitality during my visit there last summer. I would also like to thank Mr. and Mrs. Freeman, without them I will not be able to come here to Wesleyan.

I would like to thank my parents for their constant support for more than twenty years, and my sister, Saras, for always being there to chat with. Finally, I thank my housemates, fellow ST Lab thesis campers, and fellow Indonesian students at Wesleyan for keeping me cheered up during the challenging times of writing this Thesis.

# Contents

<b>1</b>	<b>Overview</b>	<b>1</b>
<b>2</b>	<b>Disordered Systems</b>	<b>4</b>
2.1	Tight-Binding Model . . . . .	5
2.1.1	Periodic Lattice . . . . .	6
2.1.2	Transfer Matrix Method . . . . .	8
2.2	Impurities . . . . .	11
2.3	Localization Length . . . . .	12
2.3.1	Definition . . . . .	12
2.3.2	Thouless Relation . . . . .	13
2.3.3	Weak Disorder Approximations of Localization Length . . . . .	15
2.4	Ring Geometries: Thin Rings and Quasi-1d Rings . . . . .	18
<b>3</b>	<b>Conductance of Mesoscopic Systems</b>	<b>21</b>
3.1	Drude Model . . . . .	22
3.2	Kubo-Greenwood Formula . . . . .	24
3.3	Diffusion-Dissipation Relation . . . . .	29
3.4	Thouless Conductance . . . . .	30
3.5	Landauer Conductance . . . . .	32
<b>4</b>	<b>Mesoscopic Conductance of Disordered Quasi-1d Rings</b>	<b>34</b>

4.1	Physical System and Modeling . . . . .	35
4.1.1	Drude Conductance . . . . .	39
4.1.2	Drude-Kubo Conductance . . . . .	40
4.1.3	SLRT: Mesoscopic Conductance . . . . .	41
4.2	Numerical Results and Analysis . . . . .	44
4.2.1	Diffusive Regime: Random Waves Conjecture . . . . .	46
4.2.2	Non-Ergodicity of Wavefunctions . . . . .	47
4.2.3	Structural Analysis of the Perturbation Operator . . . . .	49
4.3	Random Matrix Theory Modeling . . . . .	51
4.3.1	Log-Box Distribution of Matrix Elements . . . . .	52
4.3.2	Modeling Results . . . . .	53
4.3.3	Generalized Variable Range Hopping Picture . . . . .	55
4.4	Summary . . . . .	56
<b>5</b>	<b>SLRT for Systems at Metal-Insulator Transition: Preliminary Results</b>	<b>58</b>
5.1	Harper Model and Criticality . . . . .	59
5.2	Landauer Picture at Critical Point . . . . .	63
5.3	Application of SLRT: Numerical Results . . . . .	64
5.4	Fractal Structures of Perturbation Matrix . . . . .	67
5.5	Summary . . . . .	70
<b>6</b>	<b>Summary and Perspectives</b>	<b>71</b>
<b>A</b>	<b>Kramers-Kronig Relation</b>	<b>73</b>
<b>B</b>	<b>Fluctuation-Diffusion Relation</b>	<b>76</b>
<b>C</b>	<b>Connection Between Dissipation-Diffusion Relation and Kubo-Greenwood Formula</b>	<b>78</b>
<b>D</b>	<b>Hamiltonian in Adiabatic Basis</b>	<b>80</b>

# List of Figures

2.1	1d coupled pendulum system, a “mechanical analogue” to the electronic 1d tight-binding Hamiltonian. . . . .	7
2.2	Localized eigenfunction in disordered lattice with random box distribution.	13
2.3	Comparison of numerical computations and approximations of localization length for various disorders strtengths and energy values. . . . .	17
2.4	An illustration of a quasi-1d ring system. . . . .	19
3.1	Geometry used in the Landauer conductance formulation. . . . .	33
4.1	The phenomenology of energy absorption in mesoscopic rings. . . . .	37
4.2	Illustration of resistor network picture in energy space. . . . .	43
4.3	Scaled conductances $\tilde{G}_{\text{Drude}}$ , $\tilde{G}_{\text{Kubo}}$ , and $\tilde{G}_{\text{meso}}$ versus disorder strength $w$ for a quasi-1d ring with $L = 500$ and $M = 10$ . . . . .	45
4.4	Participation ratio, as a characterization of ergodicity, versus disorder $w$ for disordered quasi-1d rings in various space representations. . . . .	48
4.5	Perturbation matrix $ v_{nm} ^2$ of disordered quasi-1d rings for ballistic, diffusive, and localized regimes. . . . .	50
4.6	Bimodal distribution, an idealized distribution function for perturbation matrix elements. . . . .	51
4.7	The cumulative distribution $F(X)$ of perturbation matrix elements $X =  v_{nm} ^2$ for disordered quasi-1d ring with various values of disorder. . . . .	52

4.8	Matrix sparsity measure $p$ versus disorder strength $w$ . . . . .	54
4.9	The ratio $G_{\text{meso}}/G_{\text{Kubo}}$ versus $L/l_m = \tilde{G}_{\text{Drude}}^{-1}$ , based on the numerics of Fig. 4.3, compared with the results from the “untextured” matrices, and artificial RMT modeling using sparse matrices with log-normal or log-box distribution of matrix elements. . . . .	54
5.1	Husimi functions for the Harper model with various values of potential strength $\lambda$ , for an eigenstate that is close to the band center and $L = 377$ . . . . .	62
5.2	Plot of the energy spectrum versus $\sigma$ for the Harper model, more commonly known as Hofstadter butterfly. . . . .	63
5.3	Natural logarithm of transmission coefficient $T$ versus natural logarithm of system size $L$ for the Harper model with energy $E = 0$ and various values of $\sigma$ . . . . .	64
5.4	Scaled conductances $\tilde{G}_{\text{Drude}}$ , $\tilde{G}_{\text{Kubo}}$ , and $\tilde{G}_{\text{meso}}$ versus potential strength $\lambda$ for the Harper ring model with $L = 1000$ and $\sigma = (\sqrt{5} - 1)/2$ . . . . .	65
5.5	Scaled conductances $\tilde{G}_{\text{Drude}}$ , $\tilde{G}_{\text{Kubo}}$ , and $\tilde{G}_{\text{meso}}$ versus ring circumference $L$ for the Harper ring model at the critical point. . . . .	66
5.6	Scaled mesoscopic conductance $\tilde{G}_{\text{meso}}$ versus ring circumference $L$ for the Harper ring model for various values of $\sigma$ . . . . .	66
5.7	Different cuts of the perturbation matrix $ v_{nm} ^2$ for the Harper ring model, which shows self-similar structures. . . . .	68
5.8	Cumulative distribution $F(X)$ of perturbation matrix elements $X =  v_{nm} ^2$ for the Harper model. . . . .	69
A.1	The path of the integration of Eq. A.1 . . . . .	73

# List of Tables

2.1	Analogy between tight-binding Hamiltonian terms and coupled pendulum system terms . . . . .	7
-----	---	---

# Chapter 1

## Overview

Mesoscopic physics unifies systems with scales *between* microscopic and macroscopic. The typical sizes of these systems are of the order of nanometers. On such small scales the physics is dominated by quantum mechanics: the electrons are described by wavefunctions, with a phase which remains coherent across the system. Complex wavefunctions have both magnitude and phase—many quantum effects involve these phases. The most important quantum/wave property of electrons in the mesoscopic scale is the interference. The experimental signature of mesoscopic interference is the appearance of reproducible fluctuations in physical quantities like the conductance. The behavior and statistical properties of the conductance in various physical set-ups (for example, quantum dots, rings, or low dimensional conducting channels) was the subject of many theoretical and experimental studies during recent years [1–3].

In a typical experiment that aims to calculate the conductance of mesoscopic rings [4], a collection of mesoscopic rings are placed within a time dependent magnetic flux  $\Phi(t)$  which creates an electromotive force  $-\dot{\Phi}(t)$  in each ring. This results in an induced current which, according to Ohm's law, is  $I = -G\dot{\Phi}$ . Consequently, the energy absorption rate is given by Joule's law  $\mathcal{W} = G\dot{\Phi}^2$ , where  $G$  in this context is called the conductance. Kubo formalism for conductivity, based on *linear response theory* (LRT), has

been applied to diffusive rings [5, 6], and in this case the conductance is equivalent to that calculated using the semiclassical Drude model. Previous studies have focused on the corrections to the Drude results due to weak localization [7, 8]. These corrections do not change the leading order of Drude-Kubo results, as they are only of the order  $\Delta/\Gamma$ , where  $\Delta$  is the mean energy level spacing, and  $\Gamma$  indicates a level broadening due to environmental interactions. What happens to the Drude result if the disorder becomes weak (ballistic case) or strong (Anderson localization case)? In both cases the individual eigenfunctions become nonergodic. In the ballistic case a typical eigenfunction is not ergodic over the open modes in momentum space, while in the strong-localization case it is not ergodic over the ring in real space. A lack of quantum ergodicity implies that the perturbation matrix (current operator) is very structured and/or sparse. Consequently, the calculation of  $G$  requires a nontrivial extension of LRT. Such an extension has been proposed in [9] and later termed “semilinear response theory” (SLRT) [10]. In general, SLRT can be approached as a resistor network hopping picture [11] in energy space, which is a generalization of the real space hopping picture of [12, 13].

In this Thesis, we apply SLRT to two types of ring systems. The first system is a disordered quasi-1D ring, where we try to understand analytically the dependence of the conductance on disorder strength and sample length. The second one is the Harper Model, which is a one-dimensional system that exhibits metal-insulator transition, and shows fractality of the eigenfunctions and of the energy spectra at the critical point. We are interested in studying the nature of the conductance at the critical points, and what effect the fractal structures might have on the mesoscopic conductance.

The structure of the Thesis is as follows:

- In Chapter 2 we will discuss about disordered systems and Anderson localization in general. This includes the introduction of the mathematical model that we will use, the sources of disorder, and localization length as an observable used to quantify localization phenomena. We end this chapter by discussing modification

of our model in order to describe dirty mesoscopic rings.

- Chapter 3 deals with the methods of calculating conductance in mesoscopic systems, starting from the semiclassical Drude method, followed by Kubo formula and which is based on LRT. We also briefly mention two other methods to calculate conductance, which are the Thouless approach and Landauer formulation.
- In Chapter 4, we apply SLRT to a disordered quasi-1D ring system [14,15], where we build an analytical model to understand the departure of SLRT results from LRT in ballistic and localized regimes. We then introduce a *random matrix theory* (RMT) model based on the results of our numerical analysis on the statistical properties of the current operator matrix elements, and propose a generalization of the *variable range hopping* (VRH) estimate of the conductance. In all cases, a critical comparison between the numerical results of the Anderson ring system and of the outcomes of the theoretical modeling is performed. Important conclusions for the validity of the proposed theoretical modeling are drawn.
- In Chapter 5, we apply SLRT calculations to systems at critical conditions [16]. Specifically we study the Harper model and discuss the departure of SLRT results from Landauer and LRT results due to the emerging fractality of the eigenstates and energy spectra at critical point. This is currently a work in progress and will pave the way in understanding more realistic situations with critical behaviour, like Quantum Hall systems.
- Finally, in Chapter 6 we summarize the findings of this Thesis, and discuss numerous ideas to extend the scope of this research and the applicability of SLRT.

## Chapter 2

# Disordered Systems

In a disordered system, real space localization and absence of diffusion of a quantum particle can occur, depending on the geometry (one or higher dimensions) of the system and the strength of the disorder. This localization phenomenon was first predicted by P. W Anderson [17], hence the phenomenon is often called *Anderson localization*. Since then, Anderson localization phenomena have been studied in different types of disordered systems. The main outcome of these studies was that Anderson localization is a wave-interference phenomenon with a vast majority of applications ranging from electron motion in dirty metals to light propagation in random dielectric materials.

This chapter deals with the presentation of some fundamental ideas applied in disordered systems and Anderson localization in general. In Section 2.1 we introduce the prototype model that describes electron propagation in disordered lattices: the Anderson tight-binding model. Transfer matrix method, a numerical method that allows one to calculate the asymptotic structure of the eigenmodes of a disordered lattice, is described in Subsection 2.1.2. Section 2.2 discusses the effect of one impurity in an otherwise perfect (translationally invariant) lattice. In Section 2.3 we discuss the localization length, an observable that can be used to quantify the degree of randomness in the system and the resulting localization phenomena. The Thouless relation indicates the connection

between localization length and density of states, and is introduced in Subsection 2.3.2. Approximations of localization length for weak disorder values are discussed in Subsection 2.3.3. In Section 2.4 we close with the application of the tight-binding model to ring systems, and expand on one of the systems we will analyze in this Thesis, the quasi-1d ring, and how it is different from simple 1d rings and 2d lattices.

## 2.1 Tight-Binding Model

Below, we will work in the Wannier basis. The basis states are concentrated at individual lattice sites, making the Wannier basis a good choice for studying localization phenomena in position space. We will use *bra-ket* notation, where  $|n\rangle$  is defined as the Wannier basis state which is localized at site  $n$ . For a wavefunction  $\psi$ ,  $\langle n|\psi\rangle$  represents the amplitude of  $\psi$  at site  $n$ .

A simple model of a particle in a lattice can be given by the Hamiltonian

$$\hat{\mathcal{H}} = \sum_n \epsilon_n |n\rangle\langle n| + \sum_{\langle n,m \rangle} V_{nm} |n\rangle\langle m|, \quad (2.1)$$

where  $\langle n, m \rangle$  denotes that  $n$  and  $m$  are nearest neighbors. The first sum (the "on-site potential" terms) comes from the potential energy of atoms located at the  $n$ -th site of the lattice, and the second sum (the "nearest neighbor interaction" terms) comes from the kinetic energy terms [18]. The disorder in the system can be created by making  $\epsilon_n$  or  $V_{nm}$  random.

Now we consider the case of a 1d lattice with  $L$  sites. We assume the nearest neighbor interaction strength is constant everywhere,  $V_{nm} = V$ . The Hamiltonian of Eq. 2.1 can

be written as an  $L \times L$  matrix,

$$\mathcal{H} = \begin{pmatrix} \epsilon_1 & V & 0 & 0 & \cdots & 0 \\ V & \epsilon_2 & V & 0 & & \\ 0 & V & \epsilon_3 & V & & \vdots \\ 0 & 0 & V & \epsilon_4 & & \\ \vdots & & & & \ddots & \\ 0 & \cdots & & & & \epsilon_N \end{pmatrix}. \quad (2.2)$$

The corresponding eigenvalues and eigenvectors can be found by a direct diagonalization of the above Hamiltonian matrix.

### 2.1.1 Periodic Lattice

We consider the case of a periodic lattice, where  $\epsilon_n = \varepsilon$  for all sites. From the tight-binding Hamiltonian, we can get a set of  $L$  simultaneous equations

$$Vc_{n+1} + Vc_{n-1} + \varepsilon c_n = Ec_n, \quad (2.3)$$

where  $c_n = \langle n|\psi\rangle$  is the value of the corresponding wavefunction at site  $n$ .

In a periodic lattice, Bloch's Theorem applies (see [19]) and hence the wavefunction can be written in the Bloch form

$$c_{n+R} = c_n \exp(ikR), \quad (2.4)$$

where  $k$  is the wavenumber and  $R$  is the periodicity of the lattice. As a result, we can use the ansatz  $c_n = A \exp(inkR)$  to Eq. 2.3 to obtain

$$E = \varepsilon + 2V \cos(kR). \quad (2.5)$$

To find the possible values of  $k$ , we use hard wall boundary conditions at both ends of the lattice (sites 0 and  $L+1$ ). The phase difference ( $nkR$ ) between the two ends should

be an integer multiple of  $\pi$ , and we get the condition  $k = \frac{m}{(L+1)R}\pi$ , where  $m = 1, \dots, L$ . Finally, the energy values can be written as

$$E = \varepsilon + 2V \cos\left(\frac{m}{L+1}\pi\right). \quad (2.6)$$

It is interesting here to note the similarity between Eq. 2.3 and the discretized equations of motion of a coupled pendulum system [20],

$$m\omega_0^2 x_n - kx_{n+1} - kx_{n-1} = m\omega^2 x_n. \quad (2.7)$$

The parameters of the above equation are explained in Table 2.1, which describes the analogy between parameters of the tight-binding Hamiltonian and the coupled pendulum system. The analogy is also visualized in Fig. 2.1

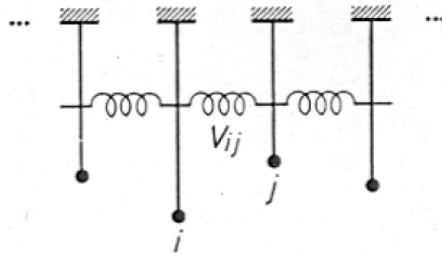


**Figure 2.1:** 1d coupled pendulum system, a “mechanical analogue” to the electronic 1d tight-binding Hamiltonian. Figure from [20]

Tight-binding Hamiltonian		Coupled pendulum system	
$c_n$ :	eigenvector component at site $n$	$x_n$ :	displacement of pendulum at site $n$
$V$ :	nearest-neighbor interaction	$-k$ :	minus spring constant between coupled sites
$E$ :	energy eigenvalue	$m\omega^2$ :	square of eigenfrequency times mass
$\varepsilon$ :	on-site potential	$m\omega_0^2$ :	square of uncoupled eigenfrequency times mass

**Table 2.1:** Analogy between tight-binding Hamiltonian terms and coupled pendulum system terms. Table adapted from Table 5.1 in [20]

Thus many of our results associated with the motion of an electron in a lattice, described by Eq. 2.3, can be easily extended to systems described by coupled oscillators (for example phononic excitations associated with the vibrations of a lattice).

### 2.1.2 Transfer Matrix Method

To find the energies and eigenvectors of the disordered system, we can diagonalize the Hamiltonian matrix of Eq. 2.2. For very large  $L$ , this will require a large amount of time and considerable computer memory, and thus can be very ineffective. In this case, *transfer matrix method* can be used instead.

Recall the sets of simultaneous equations from the previous section. Eq. 2.3 can be written in matrix form as

$$\begin{pmatrix} c_{n+1} \\ c_n \end{pmatrix} = T_n \begin{pmatrix} c_n \\ c_{n-1} \end{pmatrix}. \quad (2.8)$$

where  $T_n$  is the *transfer matrix* defined as

$$T_n \equiv \begin{pmatrix} (E - \epsilon_n)/V & -1 \\ 1 & 0 \end{pmatrix}. \quad (2.9)$$

If we consider Eqn, 2.8 from 1st site to  $n$ -th site, we can write the wavefunction for the  $n+1$ -th site as

$$\begin{pmatrix} c_{n+1} \\ c_n \end{pmatrix} = \prod_{k=1}^n T_k \begin{pmatrix} c_1 \\ c_0 \end{pmatrix}. \quad (2.10)$$

Therefore, provided that we know two components (for example  $c_0$  and  $c_1$ ) of the wavefunction for an energy value  $E$ , we can find all the remaining  $c_n$ 's by using Eq. 2.10.

As an example, we will again solve for the eigenvalues of a periodic lattice with hard wall boundary conditions (see previous subsection) using the transfer matrix method. In this case, the transfer matrix of Eq. 2.9 becomes independent of  $n$ , i.e.  $T_n = T$ . As

a result, Eq. 2.10 becomes

$$\begin{pmatrix} c_{n+1} \\ c_n \end{pmatrix} = \prod_{k=1}^n T \begin{pmatrix} c_1 \\ c_0 \end{pmatrix} = T^n \begin{pmatrix} c_1 \\ c_0 \end{pmatrix} = \begin{pmatrix} T_{11}^{(n)} & T_{12}^{(n)} \\ T_{21}^{(n)} & T_{22}^{(n)} \end{pmatrix} \begin{pmatrix} c_1 \\ c_0 \end{pmatrix}, \quad (2.11)$$

where  $T_{ij}^{(n)}$  are the matrix elements of  $T^n$ . From Eq. 2.11 we obtain an expression for  $c_{n+1}$

$$c_{n+1} = T_{11}^{(n)} c_1 + T_{12}^{(n)} c_0. \quad (2.12)$$

For a lattice of  $L$  sites, we can use the hard wall boundary condition ( $c_0 = c_{L+1} = 0$ ), which together with Eq. 2.12 results in the following relation

$$T_{11}^{(L)} c_1 = 0. \quad (2.13)$$

If  $c_1 = 0$  then we get the trivial solution i.e. all  $c_n = 0$ . This leads us to the conclusion that

$$T_{11}^{(L)} = 0. \quad (2.14)$$

Next we will solve for the nontrivial case. Let  $\alpha_1$  and  $\alpha_2$  be eigenvalues of  $T$ . Then  $\alpha_1^L$  and  $\alpha_2^L$  are eigenvalues of  $T^L$ . Also let  $\hat{x}_1$  and  $\hat{x}_2$  be the eigenvectors of  $T^L$ . Since  $T$  is a  $2 \times 2$  matrix, we can write the relation

$$T^L = d_1 T + d_0 I = \begin{pmatrix} \left(\frac{E-\varepsilon}{V}\right) d_1 + d_0 & -d_1 \\ d_1 & d_0 \end{pmatrix}, \quad (2.15)$$

where  $I$  is the identity matrix, and  $d_0$  and  $d_1$  are numbers. Using Eq. 2.15, we can write the following expression for  $T^L$ ,

$$\begin{aligned} T^L \hat{x}_1 &= \alpha_1^L \hat{x}_1 = (d_1 T + d_0 I) \hat{x}_1 = (d_1 \alpha_1 + d_0) \hat{x}_1 \\ T^L \hat{x}_2 &= \alpha_2^L \hat{x}_2 = (d_1 T + d_0 I) \hat{x}_2 = (d_1 \alpha_2 + d_0) \hat{x}_2 \end{aligned} \quad (2.16)$$

from which we can obtain the simultaneous equations

$$\begin{aligned} \alpha_1^L &= d_1 \alpha_1 + d_0 \\ \alpha_2^L &= d_1 \alpha_2 + d_0. \end{aligned} \quad (2.17)$$

These two equations have the solutions

$$\begin{aligned} d_1 &= \frac{\alpha_1^L - \alpha_2^L}{\alpha_1 - \alpha_2} \\ d_0 &= \frac{\alpha_1^L \alpha_2 - \alpha_2^L \alpha_1}{\alpha_2 - \alpha_1}. \end{aligned} \quad (2.18)$$

We can find the values of  $\alpha_i$ s by setting  $\det(T - I\alpha) = 0$  and we obtain the equation

$$\alpha^2 - \frac{E - \varepsilon}{V}\alpha + 1 = 0. \quad (2.19)$$

We also find that  $\alpha_1\alpha_2 = 1$ , and the discriminant of Eq. 2.19 is  $\left(\frac{E-\varepsilon}{V}\right)^2 - 4$ . Since a periodic lattice follows Bloch's Theorem, the  $\hat{x}$ 's need to be extended, and so the  $\alpha$ 's needs to be complex. The discriminant should be negative, and we obtain  $\left|\frac{E-\varepsilon}{V}\right| < 2$ .

As a result of this, we can use the ansatz  $\left|\frac{E-\varepsilon}{V}\right| = 2 \cos \varphi$ . Using this ansatz to find the eigenvalues of  $T$ , we obtain

$$\begin{aligned} \alpha_1 &= \exp(i\varphi) \\ \alpha_2 &= \exp(-i\varphi). \end{aligned} \quad (2.20)$$

Using this result to Eq. 2.18 we get

$$\begin{aligned} d_1 &= \frac{\sin(L\varphi)}{\sin \varphi} \\ d_0 &= -\frac{\sin[(L-1)\varphi]}{\sin \varphi}. \end{aligned} \quad (2.21)$$

Finally using the ansatz, 2.21, and the condition of Eq. 2.14 to Eq. 2.15 we obtain

$$2 \cos \varphi \frac{\sin(L\varphi)}{\sin \varphi} = \frac{\sin[(L-1)\varphi]}{\sin \varphi}. \quad (2.22)$$

This equation leads to the the following relation for  $\varphi$

$$\sin[(L+1)\varphi] = 0. \quad (2.23)$$

This results in the condition  $\varphi = \frac{m}{L+1}\pi$  where  $m = 1, \dots, L$ . If we put the condition for  $\varphi$  to the ansatz, we obtain the energy values

$$E = \varepsilon + 2V \cos\left(\frac{m}{L+1}\pi\right), \quad (2.24)$$

the same as Eq. 2.6.

We will utilize this method in Section 2.3 to derive the formula for localization length of disordered systems.

## 2.2 Impurities

In general, lattices are not purely periodic, but they can have impurities. Impurities can be caused by several factors, for example irregular spacing in the crystals, the presence of a different “species”, or other such factors. These impurities result in strong deviations from the periodic behavior.

To understand the effect of impurities, we will first consider the case of a periodic lattice with only one impurity. We consider a lattice as in Subsection 2.1.1, with  $L \rightarrow \infty$  and  $\epsilon_n = 0$  except at site  $n = 0$ , where the impurity is located,  $\epsilon_0 \neq 0$  ( $n$  goes from  $-\infty$  to  $\infty$ ). For simplicity,  $R = 1$ ,  $V = 1$ .

We recall the simultaneous equations of Eq. 2.3. For a uniform lattice (lattice with no impurities), if we use the ansatz  $c_n = A \exp(\gamma n)$  we obtain

$$[\exp(\gamma)]^2 - E \exp(\gamma) + 1 = 0. \quad (2.25)$$

For the periodic lattice case (see 2.7),  $|E| < 2$ , and the quadratic equation of Eq. 2.25 has a negative discriminant (and complex  $\exp(\gamma)$ ). Hence we can conclude that the eigenstate associated with the impurity needs to have  $|E| > 2$  (and real  $\exp(\gamma)$ ). The wavefunction needs to be normalized, so we can further assume

$$c_n = \begin{cases} A \exp(-\gamma n) & \text{if } n > 0 \\ B \exp(\gamma n) & \text{if } n < 0, \end{cases} \quad (2.26)$$

where  $\gamma > 0$ . Applying this ansatz to Eq. 2.3 for sites  $n = 1$  and  $n = -1$  gives

$$[E - \exp(\gamma)] \exp(\gamma)(A - B) = 0. \quad (2.27)$$

$\exp(\gamma) = 0$  is the trivial solution and  $\exp(\gamma) = E$  is an impossible solution since we need to have both  $|E| > 2$  and  $\exp(\gamma) < 1$ . So the only possible solution is  $A = B$ . Using this result and the fact that wavefunction should match from both positive and negative values of  $n$ , we get  $c_0 = A$ .

By applying all these requirements to Eq. 2.3 for  $n = 0$  we obtain the relation

$$E = 2 \exp(\gamma) + \epsilon_0. \quad (2.28)$$

Applying this result to Eq. 2.25 (for the remaining sites) we obtain the energy

$$E = \pm(\epsilon_0^2 + 4)^{1/2}. \quad (2.29)$$

If there is no impurity ( $\epsilon_0 = 0$ ),  $E = \pm 2$ , so the new energy is taken out from the edge of the energy spectrum of the uniform lattice. Also, it is important to note that from Eq. 2.26 the wavefunction associated with the presence of the impurity is exponentially localized at the impurity site. Thus, it is natural to expect that if we add more random impurities to the system, they will give rise to additional localized states. When all the on-site potentials have random values, we have a disordered system, and we can assume that the eigenmodes of such a system are localized and uniformly distributed over the lattice.

## 2.3 Localization Length

To find the eigenmodes of disordered systems, we can use the method described in the previous section step-by-step for each additional impurity, but this is definitely very time consuming. We can also use computational methods such as Hamiltonian matrix diagonalization, which we will use extensively in the later chapters. On the other hand, there are observables that can be used to quantify the localization phenomena. One such observable is the *localization length*.

### 2.3.1 Definition

The localization length is defined such that the localized wavefunction approximately follows the exponential relation in the  $|n| \rightarrow \infty$  limit (see the conclusion of Section

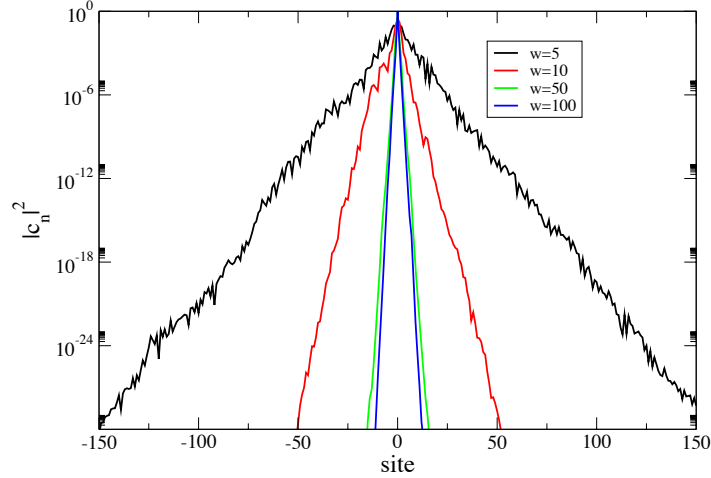


**Figure 2.2:** Localized eigenfunction in disordered lattice with random box distribution with disorder strength  $w$ . The value of  $|c_n|^2$  in the plot is the result of averaging 5 states with similar energies ( $E \approx 0$ ). The localization site is defined as the site  $n = 0$ .

2.2)

$$c_n = c_{n_0} \exp\left(-\frac{|n - n_0|}{l_\infty}\right), \quad (2.30)$$

where  $n_0$  is the site where the wavefunction is localized. The localization length itself can be written as

$$l_\infty^{-1} = -\lim_{n \rightarrow \infty} \frac{1}{|n|} \left\langle \ln \left| \frac{c_n}{c_{n_0}} \right| \right\rangle, \quad (2.31)$$

where  $\langle \dots \rangle$  means we average over different disorder realizations of the random potential.

### 2.3.2 Thouless Relation

We consider Eq. 2.10, assuming that  $c_0$  and  $c_1$  are known. For the  $N$ -th site and an energy value  $E$ , we can solve for  $c_N$  to find that  $c_N(E)$  is a polynomial of  $E$  with degree

$N - 1$

$$c_N(E) = A \prod_{n=0}^{N-1} (E - E_n), \quad (2.32)$$

where  $A$  is a constant and  $E_n$  the roots of the polynomial. Eq. 2.32 can be written as

$$c_N(E) = A \prod_{n=0}^{N-1} |E - E_n| \exp[i\pi H(E_n - E)], \quad (2.33)$$

where  $H(x)$  is the Heaviside function of  $x$ . We define

$$\Lambda(E) \equiv \lim_{N \rightarrow \infty} \frac{1}{|N|} \ln \left| \frac{c_N(E)}{c_0} \right|. \quad (2.34)$$

Using Eq. 2.33 we obtain

$$\begin{aligned} \Lambda(E) &= \frac{1}{N} \sum_n \ln |E - E_n| + \frac{i\pi}{N} \sum_n H(E_n - E) \\ &\approx \int_{-\infty}^{+\infty} dE' \rho(E') \ln |E - E'| + i\pi \int_{-\infty}^{+\infty} dE' \rho(E') H(E' - E) \end{aligned} \quad (2.35)$$

for the limit  $N \rightarrow \infty$ , where  $\rho(E)$  is the averaged density of states. We can further change the second integral of Eq. 2.35 to

$$\int_{-\infty}^{+\infty} dE' \rho(E') H(E' - E) = \int_E^{+\infty} dE' \rho(E') \equiv I(E), \quad (2.36)$$

where  $I(E)$  is defined as the integrated density of states. We can rewrite Eq. 2.35 as

$$\Lambda(E) = \int_{-\infty}^{+\infty} dE' \rho(E') \ln |E - E'| + i\pi I(E). \quad (2.37)$$

The first term is always real and the second term is always imaginary. Thus the function  $\Lambda(E)$  can be used to find the integrated density of states, and hence also the density of states by

$$I(E) = \text{Im} \left[ \frac{\Lambda(E)}{\pi} \right] \quad (2.38)$$

and

$$\rho(E) = -\frac{dI(E)}{dE}. \quad (2.39)$$

Furthermore, since the  $c_n$ 's are complex numbers they can be written as  $c_n = |c_n| \exp(i\varphi_n)$  where  $\varphi_n$  represents the phase. Substituting this into the definition of  $\Lambda(E)$  (Eq. 2.34) gives

$$\Lambda(E) = \lim_{N \rightarrow \infty} \frac{1}{N} \left[ \ln \left| \frac{c_N}{c_0} \right| + i(\varphi_N - \varphi_0) \right]. \quad (2.40)$$

Again, the first term is always real and the second term is always imaginary. The real term of Eq. 2.40 is similar to the definition of localization length of Eq. 2.31, and hence we can write the localization length as

$$l_\infty^{-1} = \text{Re}[\Lambda(E)] = \int_{-\infty}^{+\infty} dE' \rho(E') \ln |E - E'|. \quad (2.41)$$

In the above expression  $\rho(E)$  has to be understood as the average density of states  $\langle \rho(E) \rangle$ . This relation was first derived by Thouless using a Green's function formalism [21].

### 2.3.3 Weak Disorder Approximations of Localization Length

For a disordered system with a weak disorder strength, one can calculate (using perturbation theory) the resulting localization length as a function of energy and disorder potential. We consider again the simultaneous equations of Eq. 2.3, and rewrite them as

$$c_{n+1} + c_{n-1} + \lambda \epsilon_n c_n = E c_n, \quad (2.42)$$

where  $\lambda$  is a small parameter. In addition we define the ratio of the wavefunctions

$$R_n \equiv \frac{c_n}{c_{n-1}}. \quad (2.43)$$

Eq. 2.42 can then be written as

$$R_{n+1} = (E - \lambda \epsilon_n) - \frac{1}{R_n}. \quad (2.44)$$

The definition of localization length of Eq. 2.31 becomes

$$l_\infty^{-1} = \lim_{N \rightarrow \infty} \frac{1}{N} \left\langle \sum_{n=1}^N \ln |R_n| \right\rangle. \quad (2.45)$$

To find the localization length, we use the ansatz [22]

$$R_n = A \exp(\lambda B_n + \lambda^2 C_n + \lambda^3 D_n + \dots), \quad (2.46)$$

where the  $B_n, C_n, D_n, \dots$  are independent of  $\lambda$ . Applying the ansatz to Eq. 2.44, taking the Taylor expansions of  $R_{n+1}$  and  $R_n$ , and finally equating the same powers of  $\lambda$ , we obtain a set of equations

$$\lambda^0 : \quad A = E - A^{-1} \quad (2.47)$$

$$\lambda^1 : \quad AB_{n+1} = \epsilon_n - A^{-1}B_n \quad (2.48)$$

$$\lambda^2 : \quad A[C_{n+1} + \frac{1}{2}B_{n+1}^2] = A^{-1}[C_n - \frac{1}{2}B_n^2] \quad (2.49)$$

...

We need to find the values of  $A, B_n, C_n, D_n, \dots$ , averaged over multiple disorder realizations. Let us assume, without loss of generality, that  $\langle \epsilon_n \rangle = 0$  and  $\langle \epsilon_n^2 \rangle = \sigma^2$ , where  $\sigma^2$  is the variance of the disorder. From Eq. 2.47 we obtain

$$A = \frac{1}{2}[E \pm \sqrt{E^2 - 4}], \quad (2.50)$$

a constant number, and from Eq. 2.48 we obtain

$$\langle B_n \rangle = 0. \quad (2.51)$$

As shown in Eq. 2.48,  $B_n$  depends on  $\epsilon_{n-1}$  and  $B_{n-1}$ , but not to  $\epsilon_n$ , and this continues up to  $n = 1$ . Hence, we can write  $\langle \epsilon_n B_n \rangle = \langle \epsilon_n \rangle \langle B_n \rangle = 0$  to obtain

$$\langle B_n^2 \rangle = \frac{A^2}{A^4 - 1} \sigma^2, \quad (2.52)$$

and apply this to Eq. 2.49 to obtain

$$\langle C_n \rangle = -\frac{1}{2} \frac{A^2}{(A^2 - 1)^2} \sigma^2. \quad (2.53)$$

If we apply these results to Eq. 2.45 we obtain the value of the inverse localization length

$$l_\infty^{-1} = \lim_{N \rightarrow \infty} \frac{1}{N} \sum_{n=1}^N \{ \langle \ln A \rangle + \lambda \langle B_n \rangle + \lambda^2 \langle C_n \rangle + \dots \} \approx \frac{1}{2} \frac{\sigma^2}{(4 - E^2)}. \quad (2.54)$$

The disorder potentials used in the simulations that we have performed in later chapters follow a box distribution with range  $[-w/2, w/2]$ , and the variance is  $\sigma^2 = w^2/12$ . In this case the localization length becomes

$$l_\infty = 24 \frac{(4 - E^2)}{w^2}. \quad (2.55)$$

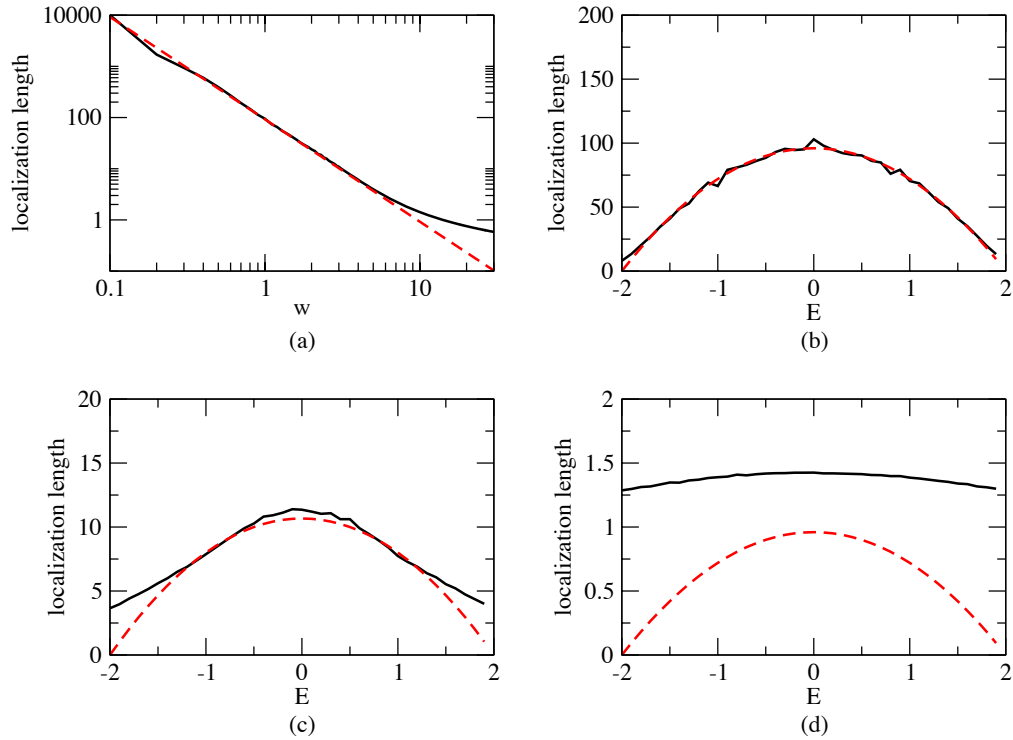


**Figure 2.3:** Numerical computations of  $l_\infty$  (solid lines) compared with the approximations of  $l_\infty$  (dashed lines) for: (a)  $w$  varied,  $E = 2 \cos(\sqrt{\pi})$ , (b)  $w = 1$ ,  $E$  varied, (c)  $w = 3$ ,  $E$  varied, (d)  $w = 10$ ,  $E$  varied.

Fig. 2.3 compares the results of this approximation with the actual localization lengths for various values of  $w$  and  $E$ . One can see a nice agreement between the numerical and perturbative results for weak disorder values, while for stronger values of the disorder deviations for the theoretical prediction Eq. 2.55 are evident. At the same time, we have

some noticeable deviations for energies at the center of the band and the band edges. These deviations were studied quite carefully in the past and their origin was identified to be related to resonance phenomena associated with rationality of the wavenumbers to the lattice periodicity [22].

## 2.4 Ring Geometries: Thin Rings and Quasi-1d Rings

The focus of this Thesis is on the analysis of the mesoscopic conductance of disordered rings in the presence of a time-dependent magnetic field. The mathematical model that describes such a physical set-up is the tight-binding Hamiltonian (Eq. 2.1) supplemented with periodic boundary conditions. The Hamiltonian matrix in the Wannier basis is written as

$$\mathcal{H} = \begin{pmatrix} \epsilon_1 & V_\phi & 0 & 0 & \cdots & V_\phi^* \\ V_\phi^* & \epsilon_2 & V_\phi & 0 & & \\ 0 & V_\phi^* & \epsilon_3 & V_\phi & & \vdots \\ 0 & 0 & V_\phi^* & \epsilon_4 & & \\ \vdots & & & & \ddots & \\ V_\phi & \cdots & & & & \epsilon_N \end{pmatrix}, \quad (2.56)$$

where  $V_\phi = V \exp(i\phi)$  and  $\phi$  is the phase of the coupling, which is contributed by the magnetic flux.

A quasi-1d ring can be constructed by stacking multiple thin rings on top of each other, and putting nearest-neighbor interaction between rings as well, effectively creating a thick ring (see Fig. 2.4). There are now two parameters for the system,  $L$ —the number of sites on each ring (or nodes), and  $M$ —the number of thin rings (or stripes), with  $L \gg M \gg 1$ . In particular, we consider the case where the nearest-neighbor interaction term is 1 between neighboring sites in the same thin ring (longitudinal), and  $c$  across thin rings (transverse). The Hamiltonian is an  $LM \times LM$  matrix but can be written as

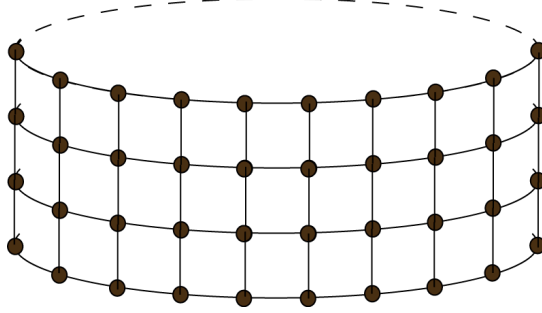


**Figure 2.4:** An illustration of a quasi-1d ring system. The dots represent the sites and the lines connecting them represent the nearest neighbor interactions.

an  $M \times M$  matrix with  $L \times L$  matrices as matrix elements

$$\mathcal{H}_{\text{quasi-1d}} = \begin{pmatrix} \mathcal{H} & C & 0 & 0 & \cdots & 0 \\ C & \mathcal{H} & C & 0 & & \\ 0 & C & \mathcal{H} & C & & \vdots \\ 0 & 0 & C & \mathcal{H} & & \\ \vdots & & & & \ddots & \\ 0 & \cdots & & & & \mathcal{H} \end{pmatrix}, \quad (2.57)$$

where  $\mathcal{H}$  is the  $L \times L$  Hamiltonian matrix for thin ring (Eq. 2.56),  $C = cI$  ( $I$  is the identity matrix), and  $0$  a matrix of all zeros.

The localization length of a quasi-1d system is different from the one of a 1d system, due to the availability of additional  $M$  propagating channels. If  $l_{\infty}^{\text{1d}}$  is the localization length of a 1d system, then according to Thouless [23], the localization length of a quasi-1d system  $l_{\infty}^{\text{quasi-1d}}$  will be

$$l_{\infty}^{\text{quasi-1d}} \approx M l_{\infty}^{\text{1d}}. \quad (2.58)$$

It is important to note that the localization length of a quasi-1d system is also different from the one of a true 2d system ( $L \sim M$ ), since in 2d systems the localization length

follows the relation [24, 25]

$$l_{\infty}^{2d} \sim \exp(1/w^2) \sim \exp(l_{\infty}^{1d}). \quad (2.59)$$

To be able to observe localization phenomena, we need the system size to be larger than the localization length, and the localization length to be larger than the mean free path of the system  $l_m$ , which is the average distance covered by the electron between subsequent scattering events. But when the system is too large, we can lose phase coherence and wave interference phenomena (which are the origin of Anderson localization) die out. For 1d systems,  $l_m \sim l_{\infty}^{1d}$ . For quasi-1d systems, from Eq. 2.58, we see that  $l_{\infty} \sim Ml_m$  while for 2d systems, from Eq. 2.59, we obtain  $l_{\infty} \propto \exp(l_m)$ . As a result, to observe localization phenomena in 1d and quasi-1d, we need a linearly increasing system size for systems with increasing mean free paths. On the other hand, we need exponentially increasing system size in 2d systems, and hence it is very hard to observe localization phenomena in 2d systems, as well as computationally ineffective. This is the reason we will not do any 2d simulations in this study.

## Chapter 3

# Conductance of Mesoscopic Systems

The response of conductors to external driving sources is a central theme in solid state theory. The advent of mesoscopic physics has brought forward questions concerning the nature of the conductance and the origin of dissipation in finite quantum coherent systems. Certain approximation schemes, which lead to satisfactory descriptions of conductors, fail in the mesoscopic regime. The present chapter will be restricted to Linear Response Theory (LRT). We will consider weakly interacting fermionic systems confined in a potential well. The independent particle picture is natural for fermion systems at low temperatures, because the low energy excitations can be modeled as independent quasi-particles [26]. One may divide the systems of interest into two types: (i) those which are coupled to the biasing source through external leads and (ii) finite conductors with no leads. There are commonly two approaches for calculating the conductance of finite quantum conductors. The first is due to Kubo and Greenwood. The second is due to Landauer. The latter was remarkably successful in accounting for the DC conductance of finite samples with leads, employing the physically appealing *scattering matrix approach*. These two approaches have been shown to be equivalent

and constitute the cornerstones of our understanding of mesoscopic transport.

The structure of this chapter is as follows: In Section 3.1 we introduce the Drude model which is the basic model used to describe the conductance of a metallic sample. Then, we will introduce the Kubo formalism and explain how one can derive in a traditional way the Kubo conductivity of a mesoscopic system. Two versions of the Kubo formula will be given: the Kubo-Greenwood formula often used in solid-state application and the Diffusion-Dissipation Relation. In the remaining part of the chapter, we briefly discuss two other methods to determine conductance. The first one is the Thouless approach, which describes the conductance in terms of the sensitivity to changes in energy eigenvalues due to small perturbations of the system. The second one is the Landauer approach mentioned above, which describes the conductance in terms of the scattering properties of the system.

### 3.1 Drude Model

Paul Drude developed a simple model to explain the transport properties of electrons in a metal. This model assumes that the positive ions are stationary, and the electrons are free to move around. The electrons are not interacting with positive ions and with each other, and follow the classical Maxwell-Boltzmann distribution.

We consider an electron in a sea of fixed scatterers (in this case, positive ions) with the mean time between collisions of electron and a scatterer to be  $\tau$ . An external electric field  $\vec{\mathcal{E}}$  is also applied to the system. Assume at time  $t$  the velocity of the electron is  $\vec{v}(t)$ . Between time  $t$  and  $t + dt$ , the probability of having a scattering event is  $\frac{dt}{\tau}$ , so the probability of not having a collision event is  $(1 - \frac{dt}{\tau})$ . If there is no collision event, the velocity of the electron will change by  $\vec{dv}$ , dictated by Newton's law  $m \frac{d\vec{v}}{dt} = \vec{F}(t) = -e\vec{\mathcal{E}}$ . If we average over all possibilities, the electron follows the equation

$$\vec{v}(t + dt) = \left(1 - \frac{dt}{\tau}\right) (\vec{v} + \vec{dv}). \quad (3.1)$$

Let us consider for simplicity a one-dimensional (1d) motion of the electrons, and use the definition  $dv = v(t + dt) - v(t)$ . Then Eq. 3.1 can be rewritten as

$$\frac{dv}{dt} = -\frac{e\mathcal{E}}{m} - \frac{v(t)}{\tau}, \quad (3.2)$$

which is equivalent to

$$m\ddot{x} + \frac{m}{\tau}\dot{x} = -e\mathcal{E}. \quad (3.3)$$

The above equation describes the motion of a particle under a constant force and a damping force which is proportional to the velocity of the electron, with a proportionality factor  $\gamma = \frac{m}{\tau}$ . After some time, a particle under these forces will reach a steady state velocity  $v_\infty$ . Steady state velocity can be determined by setting  $\frac{dv}{dt} = 0$  in Eq. 3.2.

In this case we obtain

$$v_\infty = -\frac{e\mathcal{E}}{m}\tau. \quad (3.4)$$

On average, the electrons are moving anti parallel (due to their negative charge) to the field with a velocity  $v_\infty$ . For the case of a box-shaped conductor with length  $L$ , cross-section  $A$ , and electron density  $n_e$  under an electric field  $\mathcal{E}$  parallel to its length, the current density  $j$  is

$$j = \frac{I}{A} = \frac{1}{A} \frac{dq}{dt} = -n_e e v_\infty = \left( \frac{n_e e^2 \tau}{m} \right) \mathcal{E}. \quad (3.5)$$

From Ohm's law we further have  $j = \sigma \mathcal{E}$  where  $\sigma$  is the conductivity. Direct comparison with Eq. 3.5 gives that

$$\sigma_{\text{Drude}} = \frac{n_e e^2 \tau}{m}, \quad (3.6)$$

where the mean time  $\tau$  between collisions can be written in terms of the Fermi velocity  $v_F$  and the mean free path  $l_m$  as  $\tau = l_m/v_F$ .

For a  $d$ -dimensional system, the *conductance* can be written as  $G = (L^{d-1}/L)\sigma$ . One can further evaluate the electronic density  $n_e$ , which in 1, 2, and 3-dimensions are  $n_e = 2k_F/\pi$ ,  $k_F^2/(2\pi)$  and  $k_F^3/(3\pi^2)$  (where  $k_F$  is the Fermi wavenumber) respectively.

For the 1d case, after substituting the electronic density in Eq. 3.6 and expressing  $\tau$  in terms of the mean free path, we get for the Drude conductance

$$G_{\text{Drude}} = \frac{2e^2 l_m}{\pi \hbar L}. \quad (3.7)$$

### 3.2 Kubo-Greenwood Formula

In general, the current density  $\vec{j} = (j_x, j_y, j_z)$  due to an electric field  $\vec{\mathcal{E}}$  can be written as

$$j_\alpha(\vec{r}, t) = \sum_\beta \int_0^\infty d\tau \int d\vec{r}' \sigma_{\alpha\beta}(\vec{r}, \vec{r}'; \tau) \mathcal{E}_\beta(\vec{r}', t - \tau), \quad (3.8)$$

where we used subscripts  $\alpha$  and  $\beta$  to denote Cartesian coordinate components.  $\sigma_{\alpha\beta}$  is the generalized conductivity tensor and  $\mathcal{E}_\beta$  is the  $\beta$ -component of the electric field [20].

If we consider the case of a 1d system, Eq. 3.8 becomes

$$j(x, t) = \int_0^\infty d\tau \int dx' \sigma(x, x'; \tau) \mathcal{E}(x', t - \tau). \quad (3.9)$$

An assumption that we use in this section is that the disorder is weak enough such that the localization length is much larger than the system size,  $l_\infty \gg |x|$ . Another assumption is that the electric field is homogenous,  $\mathcal{E}(x', t) \approx \mathcal{E}(t)$ . Using these two assumptions, we conclude that the current density is also homogenous,  $j(x', t) \approx j(t)$ .

The current density, averaged over  $x$  can be written as

$$\begin{aligned} \bar{j}(t) &= \langle j(t) \rangle_x = \frac{1}{V} \int dx \int_0^\infty d\tau \int dx' \sigma(x, x'; \tau) \mathcal{E}(t - \tau) \\ &= \int_0^\infty d\tau \sigma(\tau) \mathcal{E}(t - \tau), \end{aligned} \quad (3.10)$$

where  $\sigma(\tau)$  is the averaged conductivity

$$\sigma(\tau) = \frac{1}{V} \int dx dx' \sigma(x, x'; \tau). \quad (3.11)$$

We also define  $\sigma(\omega)$  as the Fourier transform of  $\sigma(\tau)$ . The relation between the two can be written as

$$\begin{aligned}\sigma(\omega) &= \int d\tau \sigma(\tau) \exp(i\omega\tau); \\ \sigma(\tau) &= \frac{1}{2\pi} \int d\omega \sigma(\omega) \exp(-i\omega\tau).\end{aligned}\quad (3.12)$$

Let us further assume that the electric field is a time-dependent monochromatic field

$$\mathcal{E}(t) = F \exp(i\omega t) + F^* \exp(-i\omega t).\quad (3.13)$$

Using Eq. 3.13 and Eq. 3.12 we can rewrite the current density of Eq. 3.10 as

$$j(t) = F \exp(-i\omega t) \sigma(\omega) + F^* \exp(i\omega t) \sigma(-\omega).\quad (3.14)$$

The current density is an observable, and hence its value must be real. This gives the condition

$$\sigma(\omega) = \sigma^*(-\omega).\quad (3.15)$$

As  $\sigma(\omega)$  is complex, we can decompose it into its real and imaginary parts,  $\sigma(\omega) = \sigma_r(\omega) + i\sigma_i(\omega)$ . By writing  $\sigma(\omega)$  in this form, we can obtain the relation for each of the components as well. Specifically we have that

$$\sigma_r(\omega) = \sigma_r(-\omega),\quad (3.16)$$

$$\sigma_i(\omega) = -\sigma_i(-\omega).\quad (3.17)$$

The above relations indicate that the real component of  $\sigma(\omega)$  is symmetric, while the imaginary component is antisymmetric.

We can find the average rate of energy dissipated by the conductor by using Joule's law

$$\begin{aligned}\langle \mathcal{W} \rangle_t &= V \langle \mathcal{E} j \rangle_t \\ &= V \langle [F \exp(i\omega t) + F^* \exp(-i\omega t)] [F \exp(-i\omega t) \sigma(\omega) + F^* \exp(i\omega t) \sigma(-\omega)] \rangle_t \\ &= V |F|^2 (\sigma(\omega) + \sigma(-\omega)) = 2V |F|^2 \sigma_r(\omega).\end{aligned}\quad (3.18)$$

where we have used the relations Eq. 3.16 and Eq. 3.17.

We can also think of the dissipated energy as the energy absorbed from the system due to all possible transitions between states,

$$\mathcal{W} = \sum_{\substack{\alpha, \beta \\ \alpha \neq \beta}} E_{\beta\alpha} \Gamma_{\alpha, \beta}, \quad (3.19)$$

where  $E_{\beta\alpha} = \hbar\omega_{\beta\alpha} = E_\beta - E_\alpha$  is the energy absorbed by the system during the field-induced transition from state  $|\alpha\rangle$  to state  $|\beta\rangle$ , and  $\Gamma_{\alpha, \beta}$  is the rate of the same transition. This transition rate  $\Gamma_{\alpha, \beta}$  can be written as

$$\Gamma_{\alpha, \beta} = f_\alpha (1 - f_\beta) \frac{dW_{\alpha\beta}}{dt}, \quad (3.20)$$

where  $f_\alpha(E_\alpha)$  and  $f_\beta(E_\beta)$  are Fermi occupation factor for states  $|\alpha\rangle$  and  $|\beta\rangle$ , respectively. ( $f_\alpha$  is the probability to be at  $|\alpha\rangle$ , and  $1 - f_\beta$  is the probability *not* to be at  $|\beta\rangle$ .) The transition probability  $W_{\alpha\beta}$  from  $|\alpha\rangle$  to  $|\beta\rangle$ , assuming a *Fermi Golden Rule* (FGR) transition, is given as (see [27, 28])

$$W_{\alpha\beta} = \left| -\frac{i}{\hbar} \int_{-\infty}^{+\infty} dt' \exp(i\omega_{\alpha\beta}t') \langle \alpha | \mathcal{H}_1 | \beta \rangle \right|^2, \quad (3.21)$$

where  $\mathcal{H}_1 = -ex\mathcal{E}$  is the Hamiltonian term that corresponds to the perturbation. Using Eq. 3.13 for the electric field, we obtain

$$\begin{aligned} W_{\alpha\beta} &= \frac{e^2}{\hbar^2} \left| \int_{-\infty}^{+\infty} dt' \exp(i\omega_{\alpha\beta}t') \langle \alpha | x (F \exp(-i\omega t') + F^* \exp(i\omega t')) | \beta \rangle \right|^2 \\ &= \frac{e^2}{\hbar^2} |\langle \alpha | x | \beta \rangle|^2 \left| F \int dt' \exp [i(\omega_{\alpha\beta} - \omega)t'] + F^* \int dt' \exp [i(\omega_{\alpha\beta} + \omega)t'] \right|^2. \end{aligned} \quad (3.22)$$

Using the definition of the delta function  $\delta(\omega - \omega') \equiv \frac{1}{2\pi} \int d\tau \exp [i(\omega - \omega')\tau]$  we can change the integral terms in Eq. 3.22 to obtain

$$\frac{dW_{\alpha\beta}}{dt} = \frac{2\pi e^2}{\hbar^2} |F|^2 |\langle \alpha | x | \beta \rangle|^2 \{ \delta(\omega - \omega_{\alpha\beta}) + \delta(\omega + \omega_{\alpha\beta}) \}. \quad (3.23)$$

We can omit one of the delta functions in the above equation. We then substitute Eq. 3.23 into Eq. 3.20. This result is then substituted into the equation for energy dissipation rate, Eq. 3.19, to obtain

$$\mathcal{W} = 2 \frac{\pi e^2}{\hbar} |F|^2 \sum_{\alpha, \beta} |\langle \alpha | x | \beta \rangle|^2 \omega_{\beta\alpha} (f_\alpha - f_\beta) \delta(\omega - \omega_{\beta\alpha}). \quad (3.24)$$

Equating Eq. 3.18 with Eq. 3.24 we can find an expression for the real component of the conductivity,

$$\sigma_r(\omega) = \frac{\pi e^2}{\hbar V} \sum_{\alpha, \beta} |\langle \alpha | x | \beta \rangle|^2 \omega_{\beta\alpha} (f_\alpha - f_\beta) \delta(\omega - \omega_{\beta\alpha}). \quad (3.25)$$

To obtain the imaginary component of the conductivity, we can use Kramers-Kronig Relation (see Appendix A)

$$\sigma_i(\omega) = -\frac{e^2}{\hbar V} \sum_{\alpha, \beta} |\langle \alpha | x | \beta \rangle|^2 \omega_{\beta\alpha} (f_\alpha - f_\beta) \frac{1}{(\omega - \omega_{\beta\alpha})}. \quad (3.26)$$

We can write the momentum operator as

$$p = m \frac{dx}{dt} = m \frac{i}{\hbar} [H, x] = m \frac{i}{\hbar} (Hx - xH), \quad (3.27)$$

and we can use this result to write  $\langle \alpha | x | \beta \rangle$ ,

$$\begin{aligned} \langle \alpha | p | \beta \rangle &= \frac{im}{\hbar} \langle \alpha | (Hx - xH) | \beta \rangle \\ &= \frac{im}{\hbar} \langle \alpha | x | \beta \rangle (E_\alpha - E_\beta) \\ \langle \alpha | x | \beta \rangle &= \frac{i}{m} \frac{\langle \alpha | p | \beta \rangle}{\omega_{\beta\alpha}}. \end{aligned} \quad (3.28)$$

Applying this result into Eq. 3.25 we obtain

$$\sigma_r(\omega) = \frac{\pi e^2}{m^2 V} \sum_{\substack{\alpha, \beta \\ \alpha \neq \beta}} |\langle \alpha | p | \beta \rangle|^2 \frac{(f_\alpha - f_\beta)}{\hbar \omega_{\beta\alpha}} \delta(\omega - \omega_{\beta\alpha}). \quad (3.29)$$

Similarly, placing Eq. 3.28 into Eq. 3.26 we get

$$\sigma_i(\omega) = -\frac{e^2}{m^2 V} \sum_{\substack{\alpha, \beta \\ \alpha \neq \beta}} |\langle \alpha | p | \beta \rangle|^2 \frac{(f_\alpha - f_\beta)}{\hbar \omega_{\beta\alpha}} \frac{1}{(\omega_{\beta\alpha} - \omega)}. \quad (3.30)$$

Electrons are fermions and hence follow Fermi-Dirac distribution. At  $T \rightarrow 0$ , the shape of the distribution is a step function and hence we can write the Fermi occupation term in Eq. 3.29 as

$$\frac{f_\alpha - f_\beta}{\hbar\omega_{\beta\alpha}} = - \left( \frac{\partial f}{\partial E} \right)_{E=E_\alpha} = \delta(E_\alpha - E_F). \quad (3.31)$$

Substituting the above expression in the relation Eq. 3.29 for the conductivity, we get

$$\sigma_r(\omega) = \frac{\pi e^2}{m^2 V} \sum_{\alpha, \beta} |\langle \alpha | p | \beta \rangle|^2 \delta(E_\alpha - E_F) \delta(\omega - \omega_{\beta\alpha}). \quad (3.32)$$

The first delta function means that we are considering electrons that are near the Fermi level. This is understandable, since due to Pauli's Exclusion Principle, only these electrons are responsible for conduction. The second delta function restricts transition between levels to those that are apart in energy by one photon.

Since we shall be interested in the behavior of finite size systems, it is worth mentioning how the sum in Eq. 3.32 can be evaluated. We consider a finitely sized system with discrete energy spectrum. The applied constant electric field is described by a harmonic vector potential in the limit  $\omega \rightarrow 0$ . A finite conductivity is the result of transitions induced by the ( $\omega$  dependent) electric field between levels separated by  $\hbar\omega$ , so that by keeping the system finite and taking the limit  $\omega \rightarrow 0$ , the conductivity vanishes. In order to obtain a finite response, two methods are usually considered. One is to take the thermodynamic limit first (for finite  $\omega$ ) so that the spectrum becomes continuous. Then, the limit  $\omega \rightarrow 0$  gives a finite conductivity. The other method, usually considered for finite-size mesoscopic systems, assumes the existence of a weak coupling between the system and external reservoirs through leads and contacts. This coupling is described phenomenologically by an energy width  $\Gamma$  over which the energy levels are spread out such that  $\hbar\omega > \Gamma > \Delta$  ( $\Delta$  being the mean level spacing), in order for the transitions between the levels to be induced by the electric field only and not by the coupling to the leads. Finally we consider the limits  $\Gamma \rightarrow 0$  and then  $\omega \rightarrow 0$ . Both methods are equivalent and represent nothing more than a way to regularize the sum in Eq. 3.32.

Keeping this in mind, one can rewrite the delta function as

$$\delta(\omega - \omega_{\beta\alpha}) \approx \frac{\hbar}{2\gamma_{\text{brd}}} \exp\left(-\frac{\hbar|\omega - \omega_{\beta\alpha}|}{\gamma_{\text{brd}}}\right), \quad (3.33)$$

where  $\gamma_{\text{brd}}$  is the broadening parameter. Taking the limits as prescribed above we obtain

$$\sigma = \frac{\pi e^2}{m^2 V} \hbar \overline{|p|^2} \rho^2, \quad (3.34)$$

where  $\rho = 1/\Delta$  is the density of states per unit energy. The above equation is called the Kubo-Greenwood formula [29, 30].

### 3.3 Diffusion-Dissipation Relation

The standard formulation of Kubo [29] takes Linear Response Theory together with thermal statistical assumptions. In this section we give another presentation which provides a more powerful picture of the conductance. Our starting point is the observation that the reversible dissipation is related to the irreversible stochastic-like diffusion in energy space induced to the system through the action of a “generalized” force. How it is possible to get dissipation (irreversible growth of the mean energy) at all, given that the up and down (in the energy spectrum) transitions are always equal? The answer is that heating is possible because the density of states  $\rho(E)$  may differ slightly at the two energies  $E = E_m \pm \hbar\omega$ , leading to a “stronger” diffusion as we go up in energy. As a result, the diffusion process is biased. Thus the average energy systematically grows with time. Lets us try to describe the evolving process of the probability distribution  $\nu(E, t)$  defined as

$$\nu(E, t) = \rho(E) f(E), \quad (3.35)$$

where  $\rho(E)$  is the density of states and  $f(E)$  is the occupation function. For large times it is argued [9] (and references therein), that the probability distribution  $\nu(E, t)$  satisfies the Fokker-Planck equation

$$\frac{\partial}{\partial t} \nu(E, t) = \frac{\partial}{\partial E} \left[ \rho(E) D_E \frac{\partial}{\partial E} \frac{\nu(E, t)}{\rho(E)} \right] \quad (3.36)$$

The average energy of the system is then  $\langle \mathcal{H} \rangle = \int dE \nu(E, t) E$  while the average rate of energy dissipation is

$$\begin{aligned} \mathcal{W} &= \frac{d\langle H \rangle}{dt} = \frac{d}{dt} \int dE E \nu(E, t) \\ &= \int dE E \frac{\partial}{\partial t} \nu(E, t) dE = \int dE E \frac{\partial}{\partial E} \left[ \rho(E) D_E \frac{\partial}{\partial E} \frac{\nu(E, t)}{\rho(E)} \right] \\ &= E \frac{\partial}{\partial E} \left[ \rho(E) D_E \frac{\partial}{\partial E} \frac{\nu(E, t)}{\rho(E)} \right] - \int \rho(E) D_E \frac{\partial}{\partial E} \frac{\nu(E, t)}{\rho(E)} dE. \end{aligned} \quad (3.37)$$

We need to have  $\nu(E, t)$  integrable (i.e.  $\int \nu(E, t) dE = N$  the number of particles in the system): at the boundaries of  $E$   $\nu(E, t) = 0$ , and thus the first term in the integration is zero. We will also assume that  $\rho(E)$  is weakly changing (for example 2D quantum dots), so

$$\mathcal{W} = - \int D_E \rho(E) \frac{\partial f(E)}{\partial E} dE. \quad (3.38)$$

The above relation is known as dissipation-diffusion equation. If we further assume that we are discussing a fermionic system, we can further substitute  $\frac{\partial f}{\partial E} = -\delta(E - E_F)$ , and  $\mathcal{W}$  can be written as

$$\mathcal{W} = D_{E_F} \rho(E_F) = \frac{1}{2} \rho(E_F) \tilde{C}(0) \dot{\Phi}^2, \quad (3.39)$$

if we use the fluctuation-diffusion relation derived in Appendix B. According to Joule's Law, the energy dissipation rate is  $\mathcal{W} = G \dot{\Phi}^2$ , where  $G$  is the conductance of the ring. Hence we obtain the conductance to be

$$G = \frac{1}{2} \rho(E_F) \tilde{C}(0). \quad (3.40)$$

The above approach allows us to consider situations where LRT does not apply. In such cases we may get some (non-perturbative) results for the diffusion, and later use the diffusion-dissipation relation in order to calculate the dissipation rate.

### 3.4 Thouless Conductance

Another widely used expression for the conductance was derived by Thouless. The main point of his argument was based on the observation that the levels of a closed sample

will respond in different ways under perturbation, depending on whether the system is in the localized or metallic regime. In this Section we present the argument of Thouless, using a mesoscopic ring in the presence of a magnetic flux as an example. We consider a ring with circumference  $L$  under an external magnetic flux  $\Phi$ . As we work in the linear response regime, we can consider  $\Phi$  to be small. We define the phase shift  $\varphi = (e/\hbar)\Phi$ . The Hamiltonian of an electron moving in the ring is

$$\begin{aligned}\mathcal{H} &= \frac{1}{2m} \left( p - \frac{e\Phi}{L} \right)^2 + V(x) \\ &= \frac{p^2}{2m} + V(x) - \frac{e\Phi}{mL} p + \frac{e^2\Phi^2}{2mL^2} \\ &\approx \mathcal{H}_0 - \frac{e\Phi}{mL} p = \mathcal{H}_0 - \frac{\hbar\varphi}{mL} p\end{aligned}\quad (3.41)$$

where  $\mathcal{H}_0$  is the Hamiltonian when there is no flux, and we can omit the  $\Phi^2$  term.

The first-order energy shift is given by the perturbation theory  $E_\beta^{(1)} = -\frac{\hbar\varphi}{L} \langle \beta | p | \beta \rangle$ , but as the momentum operator matrix has zero diagonal elements,  $E_\beta^{(1)} = 0$ . The second-order energy shift is given by

$$E_\beta^{(2)} = \left( \frac{\hbar\varphi}{mL} \right)^2 \sum_{\alpha \neq \beta} \frac{|\langle \alpha | p | \beta \rangle|^2}{E_\beta^{(0)} - E_\alpha^{(0)}}. \quad (3.42)$$

The energy levels  $E(\varphi)$  can also be written as a Taylor expansion around  $\varphi = 0$ :  $E(\varphi) = E(0) + E'(0)\varphi + E''(0)\frac{\varphi^2}{2} + \dots$ . By equating the quadratic term with 3.42 we obtain

$$E_\beta''(0) = 2 \frac{\hbar^2}{m^2 L^2} \sum_{\alpha \neq \beta} \frac{|\langle \alpha | p | \beta \rangle|^2}{E_\beta^{(0)} - E_\alpha^{(0)}}. \quad (3.43)$$

Assuming now that the sum  $\sum \frac{1}{E_\beta^{(0)} - E_\alpha^{(0)}}$  is dominated by the smallest  $E_\beta^{(0)} - E_\alpha^{(0)}$  which is of order  $\sim \Delta$  and replacing  $|\langle \alpha | p | \beta \rangle|^2$  by its characteristic value  $\overline{|p|^2}$ , we obtain

$$\overline{|E_\beta''(0)|} \sim \frac{\hbar^2}{m^2 L^2} \overline{|p|^2} \rho. \quad (3.44)$$

The Thouless energy  $E_T$  is defined as  $E_T \equiv \overline{|E''(0)|}$ . Using Kubo-Greenwood formula of Eq. 3.34, the conductance can be written as

$$G \sim \frac{e^2}{\hbar} \frac{E_T}{\Delta}. \quad (3.45)$$

This relation was derived for the first time by Thouless [31, 32], and it shows the dependence of conductance on mean level spacing, and the sensitivity to the changes in energy eigenvalues due to perturbations.

### 3.5 Landauer Conductance

Landauer's approach assumes that the mesoscopic sample is attached to leads, and employs the scattering matrix formalism. Economou and Soukoulis showed that under appropriate circumstances it is equivalent to the Kubo-Greenwood results for conductance [33]. Specifically, in contrast to the Kubo formalism it addresses only the DC response and cannot incorporate leadless geometries. Nevertheless, during the last 25 years this method has received much attention and many interesting results were derived using this approach. Below we review the main ideas underlying this method.

Landauer first developed this formulation for one-dimensional systems. Let us assume a system with transmission coefficient  $T$  and reflection coefficient  $R = 1 - T$ . The system is connected by perfectly conducting wires to some external current source  $I$ . The conductance is defined as  $I/V$ , where  $V$  is the voltage across the conductor, and can be written [34, 35] as

$$G = \frac{e^2}{\pi\hbar} \frac{T}{(1-T)}. \quad (3.46)$$

Clearly, this first result of Landauer was problematic since in the limit of a perfect conductor  $T \rightarrow 1$  it gives  $G \rightarrow \infty$ .

Economou and Soukoulis corrected Landauer's formulation using the Kubo formalism and obtained the conductance [33, 36] as

$$G_c = \frac{e^2}{\pi\hbar} T. \quad (3.47)$$

Unlike Eq. 3.46,  $G_c$  in Eq. 3.47 has a finite value for all possible values of  $T$ , and  $G_c < G$ , except when  $T = 0$ .

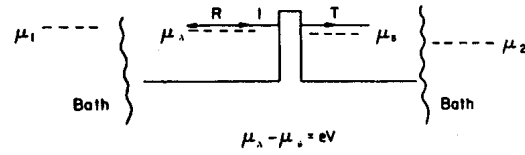


**Figure 3.1:** Geometry used in the Landauer conductance formulation: a system of scatterers connected to a pair of reservoirs.  $\mu_A$  and  $\mu_B$  are the chemical potentials of the ends of the scatterer, and  $\mu_1$  and  $\mu_2$  are the chemical potentials of the baths. Figure from [37].

Another way to view the difference between the two formulations is described in [37]. Consider a scatterer system connected to two reservoirs, one at each end, and the waves are coming from the two reservoirs (see Fig. 3.1). Eq. 3.46 measures the conductance *between the two ends of the scatterer*, which is given by  $G = I/(\mu_A - \mu_B)$ , where  $\mu_A$  and  $\mu_B$  are the chemical potentials of each end of the scatterer. Meanwhile, Eq. 3.47 measures the conductance *between the two reservoirs*, which have chemical potentials  $\mu_1$  and  $\mu_2$ , and the conductance is given by  $G_c = I/(\mu_1 - \mu_2)$ .

## Chapter 4

# Mesoscopic Conductance of Disordered Quasi-1d Rings

In this chapter we present a theoretical and numerical analysis [14,15] of the conductance of mesoscopic rings using *semilinear response theory* (SLRT). We begin our presentation by describing the physical system under consideration, and discuss the assumptions underlying this study. Section 4.2 details the calculation method used to determine the conductance, for semiclassical (Drude), LRT (Kubo), and SLRT methods. In Section 4.3 we focus on quasi-1d rings. Here we show the dependence of the conductance on the disorder strength and compare the outcomes of SLRT with the results of the traditional Kubo formalism. Following this, we build an analytical model to understand the departure of SLRT results from LRT results in ballistic (weak disorder) and localized (strong disorder) regimes. In Section 4.4 we introduce a *random matrix theory* (RMT) model with log-box and log-normal distributed elements, based on the sparsity of the numerical results, and a generalized *variable range hopping* (VRH) estimate of the conductance, and discussing the applicability of these models by comparing them with the numerical results. This chapter ends with the summary of our findings.

## 4.1 Physical System and Modeling

A typical experiment that aims to measure the conductance of mesoscopic rings is described in [4], where an ensemble of mesoscopic rings are placed under a perpendicular (to the plane of the ring) time-dependent magnetic flux  $\Phi$ . The induced (according to Faraday’s law) electromotive force (EMF)  $-\dot{\Phi}$  results in a current which, according to Ohm’s law is  $I = -G\varepsilon$  ( $\varepsilon = \dot{\Phi}$  is the voltage). The dissipated energy can either be accumulated by the electrons (as kinetic energy), or it may be eventually transferred to the lattice vibrations. In the latter case the ring is “heated”. The rate of heating (rate of energy absorption) is given by Joule’s law

$$\mathcal{W} = G\varepsilon^2. \quad (4.1)$$

where  $G$  is the “conductance” (inverse resistance) of the ring. This definition of conductance was also used in [4,38].

We will assume low frequency noisy driving with a power spectrum

$$\tilde{F}(\omega) = \varepsilon^2 \frac{1}{2\gamma_{\text{brd}}} \exp\left(-\frac{\hbar|\omega|}{\gamma_{\text{brd}}}\right) \equiv \varepsilon^2 \delta_{\gamma_{\text{brd}}}(\hbar\omega), \quad (4.2)$$

where  $\varepsilon$  is the root-mean-square value of the voltage and  $\gamma_{\text{brd}}$  is the broadening parameter of the spectrum. We want  $\gamma_{\text{brd}}$  to be small enough compared to any relevant semiclassical energy scale to avoid the semiclassical limit, but large enough compared to the mean level spacing  $\Delta$  in order to avoid quantum recurrences that might appear in strictly linear or periodic driving. Alternatively, if we use the assumption of an interaction with the environment or an external thermal bath, we will get a similar result and the parameter  $\gamma_{\text{brd}}$  can be extracted from the level broadening or temperature of the bath (see Section 3.2).

In “mesoscopic” circumstances, we assume that the coherence time of the system is much longer than the ballistic time (the time required by waves to propagate through the system), but shorter than the Heisenberg time ( $\hbar/\Delta$ ). We will also assume that the

system can release energy to some external bath, resulting in a “heat flow” with rate  $\mathcal{Q}$ , governed by the relaxation rate  $\gamma_{\text{rlx}}$  towards the equilibrium. The system reaches steady state when  $\mathcal{Q} = \mathcal{W}$ . The two energy scales  $\gamma_{\text{brd}}$  and  $\gamma_{\text{rlx}}$  describe different physics. The former is essential in order to analyze the induced FGR transitions between levels and as such it directly affects the energy absorption rate  $\mathcal{W}$ , while the latter is responsible for achieving a steady state. The overall physical picture of the energy absorption is shown by Fig. 4.1(a).

Let us assume that the ensemble of rings possesses broad thermal population of energy levels. Some of the rings will have a higher absorption rate than others, depending on the coupling strength of the initial level to its neighboring levels. The *initial* rate of the energy absorption (per ring) is then obtained by a simple *algebraic* averaging of the absorption rates of each individual ring  $\langle \mathcal{W} \rangle$ . This algebraic averaging reflects the statistical nature of the preparation and has nothing to do with the nature of the dynamics [9].

Generally, when we measure the conductance we are not interested in the transient behavior but in the long term behavior. The transient behavior is characterized by a time scale  $t_{\text{stbl}}$ . In [9] it is shown that  $t_{\text{stbl}}$  depends on the EMF:  $t_{\text{stbl}}$  decreases with increasing  $\varepsilon$ . For  $t \ll t_{\text{stbl}}$  the absorption rate depends on the probability to make *long sequences of transitions*. In the long term behavior, the absorption will slow down and the conductance will be smaller when compared with the initial conductance. If we take the relaxation process into account, two possible scenarios are possible, as illustrated in Fig. 4.1(b). The first possibility occurs when the relaxation is weak,

$$\gamma_{\text{rlx}}^{-1} \gg t_{\text{stbl}}/\hbar, \quad (4.3)$$

where the absorption will slow down as in the previous case. The other possibility happens if we have relaxation that is strong enough to mask the intrinsic dynamics of the system. This condition can also be achieved if  $\varepsilon$  is small such that Eq. 4.3 breaks down. In this case, the relaxation process returns the level distribution to its initial

state before the slow down can occur, and there is no drop in the conductance value [9]. Here we will assume the former case of weak relaxation, and we call the conductance based on this assumption the *mesoscopic conductance*.

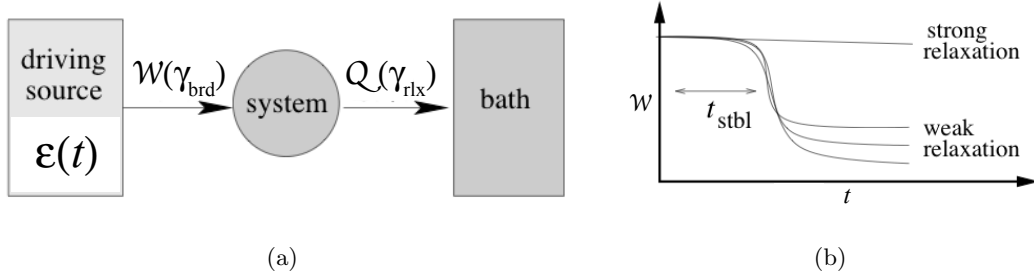


**Figure 4.1:** The phenomenology of energy absorption in mesoscopic rings. In (a) we highlight the energy processes in the ring: energy absorption  $\mathcal{W}$ , which depends on the level broadening parameter  $\gamma_{\text{brd}}$ , and heat flow  $\mathcal{Q}$ , which depends on the relaxation rate  $\gamma_{\text{rlx}}$ . In (b) we show how  $\mathcal{W}$  depends on time. If  $\gamma_{\text{rlx}}$  is small then there is a transient leading to a slower absorption rate that depends on  $\gamma_{\text{brd}}$ . Figure from [9].

Kubo conductivity, based on *linear response theory* (LRT) has been applied to diffusive rings [5, 6], and in this case we get the Drude results. In Section 3.2 we show that the Kubo conductance can be obtained by performing an algebraic averaging of the perturbation matrix elements, which is proportional to the absorption rates between levels. This result is to be expected since the underlying assumption of Kubo is that the system is always near equilibrium.

Previous studies have focused on the corrections to the Kubo-Drude results due to weak localization [7, 8]. These corrections do not change the leading order of the Kubo-Drude results, as they are only of the order  $\Delta/\gamma_{\text{brd}}$ . In the strong disorder limit there are two conflicting results for the  $\gamma_{\text{brd}}$  dependence of conductance, both based on Mott's work [39, 40]. On the basis of the Kubo formula, one expects  $G \sim \gamma_{\text{brd}}^2 |\log(\gamma_{\text{brd}})|^{d+1}$  where  $d=1$  for quasi one-dimensional (quasi-1d) ring. While on the basis of the variable range hopping (VRH) phenomenology, one expects  $G \sim \exp(-(\gamma_0/\gamma_{\text{brd}})^{1/(d+1)})$ , where  $\gamma_0$  is a constant.

Here, we will show that a novel unified framework termed *semilinear response theory* (SLRT), originally introduced in [9] and further extended in [10], can be used to describe equivalently the ballistic (weak disorder), diffusive, and localized (strong disorder) regimes. In the LRT limit, SLRT leads to LRT, while in general for mesoscopic conditions SLRT can be approached as a resistor network hopping picture [11] in energy space, which is a generalization of the real space hopping picture of [12, 13].

We consider the case of a quasi-1d ring with circumference (number of nodes)  $L$  and number of channels  $M$ . Each site in the ring has random potential given by a box distribution of width  $w$ . The nearest neighbor coupling term in the longitudinal direction is  $c_{\parallel} = 1$ , while in the transverse direction it is  $c_{\perp} = c < 1$ . We will also use natural units such that  $\hbar = 1$  and the mass of the electron  $m_e = 1$ .

As we have shown in Section 3.2, the perturbation operator associated with the perpendicular magnetic field is the current operator  $I$ , which is proportional to the velocity operator  $\hat{v}$ . For thin rings, we can write the corresponding velocity operator  $\hat{v} = -(i\hbar/m)(\partial/\partial x)$  in the Wannier basis

$$v_{1D} = \frac{i\hbar}{2m_e} \begin{pmatrix} 0 & -1 & 0 & 0 & \cdots & 1 \\ 1 & 0 & -1 & 0 & & \\ 0 & 1 & 0 & -1 & & \vdots \\ 0 & 0 & 1 & 0 & & \\ \vdots & & & & \ddots & \\ -1 & \cdots & & & & 0 \end{pmatrix}. \quad (4.4)$$

For a quasi-1d ring system, assuming current only flows in longitudinal direction, the current matrix in position basis can be written as an  $M \times M$  matrix with  $L \times L$  matrices

as matrix elements

$$v_{\text{quasi-1D}} = \begin{pmatrix} v_{1\text{D}} & 0 & 0 & \cdots & 0 \\ 0 & v_{1\text{D}} & 0 & & \\ 0 & 0 & v_{1\text{D}} & & \vdots \\ \vdots & & & \ddots & \\ 0 & & \cdots & & v_{1\text{D}} \end{pmatrix}. \quad (4.5)$$

In our simulations, we compute the scaled conductance defined as

$$\tilde{G} = \frac{G}{(e^2/2\pi\hbar)M}. \quad (4.6)$$

In the case of systems with open (Landauer) geometries,  $\tilde{G}$  is the average transmission per channel. For closed (ring) geometries,  $\tilde{G}$  depends on the structure and the sparsity of the perturbation matrix.

#### 4.1.1 Drude Conductance

Drude conductance of the ring can be obtained from the single-channel results of Section 3.1 by applying them to a multichannel system. In the case of one dimensional systems, using Green's function formalism one can find the relation between mean free path  $l_m$  and localization length  $l_\infty$  [20] to be

$$l_\infty = 4l_m. \quad (4.7)$$

For quasi-1d systems, we have  $l_\infty \sim Ml_m$  (see section 2.4). If we apply these relations to Eq. 3.7 we obtain the Drude conductance

$$G_{\text{Drude}} = \frac{e^2}{2\pi\hbar} M \frac{l_m}{L}. \quad (4.8)$$

Here the Drude scaled conductance  $\tilde{G}_{\text{Drude}}$  is just the ratio between the mean free path and the circumference of the ring.

From Subsection 2.3.3 we find that the localization length of a 1d system, and hence also the mean free path, is approximately proportional to  $(4 - E^2)/w^2$ . For periodic lattices  $E = 2 \cos k$ , where  $k$  is the wavenumber, and so  $l_m \sim [2 \sin k/w]^2$ . The velocity of the electrons at the Fermi level is given by  $v_F = \partial E / \partial k|_{E=E_F} = 2 \sin k$ . The mean free path is then

$$l_m \sim \left(\frac{v_F}{w}\right)^2. \quad (4.9)$$

We can write the total number of states  $N$  in terms of energy  $E$  as

$$N = \frac{ML}{\pi \hbar} \sqrt{2mE}, \quad (4.10)$$

where in our case, the volume of the system is  $ML$ . The density of states can be obtained by taking the derivative

$$\rho(E) = \frac{dN}{dE} = \frac{ML}{\pi \hbar} \sqrt{\frac{m}{2E}} = \frac{ML}{\pi \hbar v(E)}. \quad (4.11)$$

The density of states is equivalent to the inverse of the spacing between energy levels  $\Delta$ . At the Fermi level, the density of states is then

$$\rho_F = \rho(E_F) = \frac{ML}{\pi \hbar v_F} \equiv \frac{1}{\Delta}. \quad (4.12)$$

By applying Eq. 4.9 and Eq. 4.12 to Eq. 4.8, we obtain the expression for the scaled conductance

$$\tilde{G}_{\text{Drude}} \sim \frac{M^2 L \Delta^2}{\pi^2 \hbar^2 w^2}. \quad (4.13)$$

### 4.1.2 Drude-Kubo Conductance

The Diffusion-Dissipation Relation derived in Section 3.3 gives

$$G = \frac{1}{2} \rho(E_F) \tilde{C}(0). \quad (4.14)$$

We can obtain the Drude conductance of the previous subsection by using the following classical approximation

$$C(t) = \left(\frac{e}{L}\right)^2 \langle v(t) v(0) \rangle \approx \left(\frac{e}{L}\right)^2 v_F^2 \exp\left[-2\frac{v_F}{l_m}|t|\right], \quad (4.15)$$

and applying the Fourier transform of the above equation to Eq. 4.14.

On the other hand, if we take quantum effects into account, by substituting  $\tilde{C}(\omega)$  from Appendix C and the broadened delta  $\delta_{\gamma_{\text{brd}}}$  to Eq. 4.14 we obtain

$$\begin{aligned} G_{\text{Kubo}} &= \pi\hbar \left(\frac{e}{L}\right)^2 \rho_F \frac{1}{N} \sum_{n,m} |v_{nm}|^2 \delta_{\gamma_{\text{brd}}}(E_m - E_n) \\ &\equiv \pi\hbar \left(\frac{e}{L}\right)^2 \rho_F^2 \langle\langle |v_{nm}|^2 \rangle\rangle, \end{aligned} \quad (4.16)$$

where the average is over  $N$  nearby open mode states within a chosen energy window.

The spectral function  $\tilde{C}(\omega)$  is the Fourier transform of the current-current correlation function, and can be re-interpreted as the band profile of the perturbation matrix in the eigenvalue basis. The weak localization corrections are determined by the interplay of the broadened delta function with the level statistics. One important thing to note is that  $\langle\langle \dots \rangle\rangle_{\text{LRT}}$  in Eq. 4.16 is a simple *algebraic* average over nearby diagonal matrix elements within the chosen energy window.

The scaled conductance is then

$$\tilde{G}_{\text{Kubo}} = 2\pi^2\hbar^2 \frac{1}{ML^2} \frac{1}{N\Delta} \sum_{n,m} |v_{nm}|^2 \delta_{\gamma_{\text{brd}}}(E_m - E_n). \quad (4.17)$$

### 4.1.3 SLRT: Mesoscopic Conductance

Similar to the derivation of Kubo conductance, also in the SLRT we use the assumption that the energy absorption is dominated by FGR transitions. As shown before, the transition rate in FGR transitions is proportional to the squared matrix element  $|v_{nm}|^2$  of the velocity operator. Because the absorption rate highly depends on the probability to make *connected* transitions, SLRT [9] does not directly lead to Kubo formula. Both the structure and the sparsity of the  $|v_{nm}|^2$  matrix have significant effects on the conductance  $G$ . The main outcome of SLRT is that the conductance formula can be

written in the form of Eq. 4.16, where we have the scaled conductance

$$\tilde{G} = \frac{2M}{v_F^2} \langle\langle |v_{nm}|^2 \rangle\rangle, \quad (4.18)$$

but with a modified definition of  $\langle\langle \dots \rangle\rangle$ —which is now not an averaging but something different based on resistor network picture calculation. It was shown in [9, 41] that  $\langle\langle \dots \rangle\rangle$  is bounded from above by *algebraic* averaging  $\langle X \rangle$ , and from below by *harmonic* averaging  $\langle X^{-1} \rangle^{-1}$ . In the remaining part of this subsection we will describe the details of SLRT conductance calculations.

We again consider the Hamiltonian of a ring system under magnetic flux, introduced in Section 3.3,  $\mathcal{H} = \mathcal{H} + \Phi I$ . To calculate the mesoscopic conductance (Eq. 4.18), we will work in the adiabatic basis, where the basis vectors are the instantaneous eigenvectors of the Hamiltonian  $\mathcal{H}$ . The Hamiltonian matrix elements can be written in the adiabatic basis (see Appendix D for derivation) as

$$\mathcal{H}_{nm} = E_n \delta_{nm} + \dot{\Phi} V_{nm}. \quad (4.19)$$

where  $E_n$  are the instantaneous eigenvalues and

$$V_{nm} = i\hbar \frac{I_{nm}}{(E_n - E_m)}. \quad (4.20)$$

We can write the FGR transition probability from states  $|n\rangle$  to  $|m\rangle$  as (see [27, 28])

$$W_{nm} = \left| -\frac{i}{\hbar} \int_{-\infty}^{+\infty} dt' e^{i\omega_{nm}t'} \langle n | \dot{\Phi} V | m \rangle \right|^2. \quad (4.21)$$

Then we can write the rate of energy absorption between the same states as

$$\Gamma_{n,m} = \frac{2\pi}{\hbar} \rho |V_{nm}|^2 \dot{\Phi}^2. \quad (4.22)$$

The transition can only occur when the energy absorbed equals the energy difference between the two states, so we can approximate the density of state as a delta function peaked at the energy difference,  $\rho \approx \delta_{\gamma_{\text{brd}}}(E_m - E_n)$ .

The energy absorption rate from the FGR transition between states  $|n\rangle$  and  $|m\rangle$  of Eq. 4.22 (based on Joule's Law) equals  $G_{nm}\dot{\Phi}^2$ , where  $G_{nm}$  is the conductance (inverse resistance) between the two states

$$G_{nm} = \frac{2\pi}{\hbar} |V_{nm}|^2 \delta(E_n - E_m) = 2\pi\hbar \left(\frac{e}{L}\right)^2 \frac{|v_{nm}|^2}{(E_n - E_m)^2} \delta(E_n - E_m). \quad (4.23)$$

Instead of  $G_{nm}$ , we will work with the scaled conductivity between two states  $g_{nm}$ , defined as

$$g_{nm} = 2\Delta^3 \frac{|v_{nm}|^2}{(E_n - E_m)^2} \delta(E_n - E_m), \quad (4.24)$$

related to  $G_{nm}$  as

$$G_{nm} = \frac{\pi\hbar}{\Delta^3} \left(\frac{e}{L}\right)^2 g_{nm}. \quad (4.25)$$

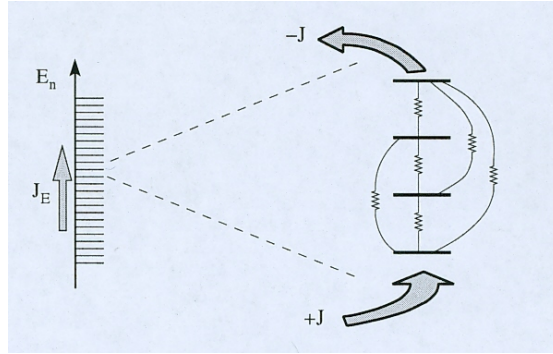


**Figure 4.2:** Illustration of resistor network picture in energy space. The resistance of a "resistor" connecting states  $n$  and  $m$  corresponds to  $g_{nm}^{-1}$ . The right side of the image shows a truncated segment of the network, with current  $J$  goes into one end and the same current  $J$  exits another end, while the net current in other sites is zero. Figure from [41].

The following method is adapted from [41]. We consider a resistor network of  $N$  sites in the energy space. We assume that current with strength  $J$  goes into one end (we use the state with the lowest energy), and the same current strength  $J$  exits another end (we use the state with the highest energy), and in the remaining sites there is zero net current. Hence we can represent the injected current in the network as a vector  $\mathbf{J} = (J_1, J_2, \dots, J_N)$ , with all zero elements except  $J_1 = +J$  and  $J_N = -J$ .

We can then use Kirchoff's laws to relate the current and potential in the network

$$J_n = \sum_m g_{nm}(V_m - V_n) = \left( \sum_m g_{nm} V_m \right) - \left( \sum_m g_{nm} \right) V_n, \quad (4.26)$$

where  $V_n$  is the potential of site  $n$ . For all  $N$  sites, Eq. 4.26 can be represented as a matrix multiplication

$$\mathbf{J} = g' \mathbf{V}, \quad (4.27)$$

where  $\mathbf{V} = (V_1, V_2, \dots, V_N)$  and  $g'$  has matrix elements

$$g'_{nm} = g_{nm} - \left( \sum_k g_{km} \right) \delta_{nm}. \quad (4.28)$$

Using Eq. 4.27, we find

$$\mathbf{V} = (g')^{-1} \mathbf{J}. \quad (4.29)$$

The conductance of the *whole* resistor network is

$$g_N = \frac{J}{V_N - V_1}. \quad (4.30)$$

We then define the conductance of the ring as  $g = N g_N$ .

The mesoscopic conductance  $G_{meso}$  can be written as

$$G_{meso} = \frac{\pi \hbar}{\Delta^3} \left( \frac{e}{L} \right)^2 g = \frac{\pi \hbar}{\Delta^3} \left( \frac{e}{L} \right)^2 \frac{NJ}{(V_N - V_1)}, \quad (4.31)$$

and the scaled conductance  $\tilde{G}_{meso}$  can be written as

$$\tilde{G}_{meso} = 2\pi^2 \hbar^2 \frac{1}{ML^2} \frac{1}{\Delta^3} \left( \frac{NJ}{V_N - V_1} \right). \quad (4.32)$$

## 4.2 Numerical Results and Analysis

For a quasi-1d ring of  $L = 500$  and  $M = 10$ , the plots of scaled conductances  $\tilde{G}_{\text{Drude}}$  (Eq. 4.13),  $\tilde{G}_{\text{Kubo}}$  (Eq. 4.17), and  $\tilde{G}_{\text{meso}}$  (Eq. 4.32) are shown in Fig. 4.3. We observe departure of the SLRT conductance ( $\tilde{G}_{\text{meso}}$ ) results from Drude-Kubo results in the weak disorder (ballistic) and strong disorder (localized) regimes.

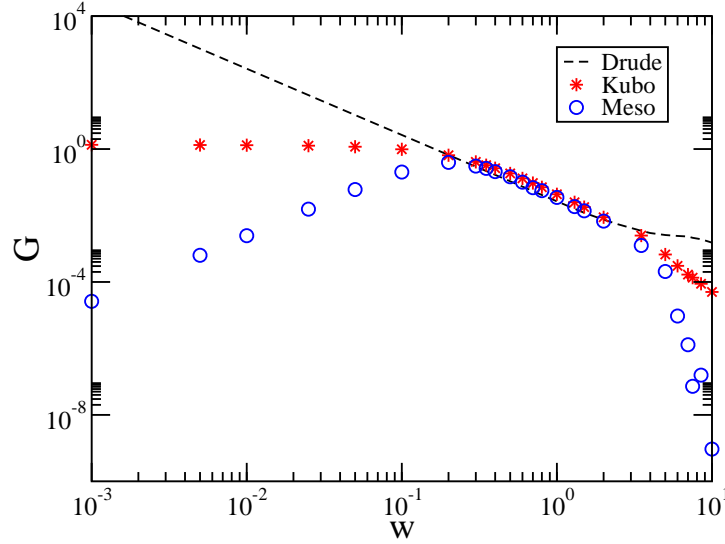


**Figure 4.3:** Scaled conductances  $\tilde{G}_{\text{Drude}}$ ,  $\tilde{G}_{\text{Kubo}}$ ,  $\tilde{G}_{\text{meso}}$  versus disorder strength  $w$  for a quasi-1d ring with  $L = 500$  and  $M = 10$ , transverse nearest neighbor interaction  $c = 0.9$ , and broadening parameter  $\gamma_{\text{brd}}/\Delta = 7$ . Figure from [14].

In order to determine numerically whether the structure of the matrix is of any importance, we permute randomly the elements of the  $v_{nm}$  matrix along the diagonals (the “untextured” matrix) and recalculate  $\tilde{G}$ . By definition,  $G_{\text{Kubo}}$  is not affected by this procedure. We find that  $G_{\text{meso}}$  is slightly affected by this in the ballistic regime, but the qualitative results are generally the same. Accordingly, we deduce that the main issue is the *sparsity*, and concentrate below on the RMT modeling of sparsity.

In the rest of this section, we will construct an analytical model of the ring that will help us to understand the numerical results. We will start with the discussion of the diffusive regime, where LRT, SLRT, and also semiclassical approximations are all in agreement. Then we will continue with the discussion of the ballistic and localized regimes, where we observe departures (see Fig. 4.3) of the SLRT results from the LRT results. The departures correspond to the non-ergodicity of the wavefunctions.

### 4.2.1 Diffusive Regime: Random Waves Conjecture

In the diffusive regime, Mott has argued that the eigenstates of the Hamiltonian matrix are ergodic in position space, and look like random waves [39, 40]. Using this assumption one can reconstruct the Drude result. Following Mott, we assume that  $l_m$  is the correlation scale of any typical wavefunction  $\Psi(x, y)$ . The total volume  $L^d$  is divided into domains of size  $l_m^d$ , and hence we have  $(L/l_m)^d$  such domains.

Next we will consider the quasi-1d case where  $d = 1$ . Using the definition of the velocity operator, the velocity matrix elements can be written as the integral

$$v_{nm} = \langle n|v|m\rangle = \frac{\hbar}{im_e} \int dx \psi_n^*(x) \frac{d}{dx} \psi_m(x), \quad (4.33)$$

where  $\psi_n(x)$  is the wavefunction of state  $|n\rangle$  in real space. If we use Mott's assumption, the integral can be written as separate integrals for each domain, and Eq. 4.33 becomes

$$v_{nm} = \frac{\hbar}{im_e} \sum_a^{L/l_m} \int_{l_a} dx \psi_n^*(x) \frac{d}{dx} \psi_m(x), \quad (4.34)$$

where  $l_a$  is the integration path within a domain  $a$ . The perturbation matrix elements  $|v_{nm}|^2$  are then given by

$$|v_{nm}|^2 = \left| \frac{\hbar}{im_e} \sum_a^{L/l_m} \int_{l_a} dx \psi_n^*(x) \frac{d}{dx} \psi_m(x) \right|^2 = \left( \frac{\hbar}{m_e} \right)^2 \left| \sum_a^{L/l_m} \mathcal{I}_a(l_a) \right|^2, \quad (4.35)$$

where we have defined

$$\mathcal{I}_a(l_a) \equiv \int_{l_a} dx \psi_n^*(x) \frac{d}{dx} \psi_m(x). \quad (4.36)$$

The sum term in Eq. 4.35 can be written as

$$\left| \sum_a^{L/l_m} \mathcal{I}_a(l_a) \right|^2 = \sum_a^{L/l_m} |\mathcal{I}_a(l_a)|^2 + \text{cross terms}. \quad (4.37)$$

If we average over different disorder realizations, due to uncorrelated velocities the cross terms will go to zero. Assuming further that  $\mathcal{I}_a(l_a) \approx \mathcal{I}$  we finally get the following

expression for the velocity matrix elements

$$|v_{nm}|^2 = \left(\frac{\hbar}{m_e}\right)^2 |\mathcal{I}|^2 \frac{L}{l_m}. \quad (4.38)$$

Mott uses the assumption that locally the eigenstates are similar to free waves, and hence  $\psi(x) \approx \exp(ikx)$ . We can then evaluate  $\mathcal{I}$ ,

$$\begin{aligned} \mathcal{I}_a(l_a) &\approx \int_{l_a} dx \exp(-ik_n x) \frac{d}{dx} \exp(ik_m x) \\ &= ik_m \int_{l_a} dx \exp[-i(k_n - k_m)x] \\ &\approx ik_F \overline{|\psi|^2} l_m, \end{aligned} \quad (4.39)$$

since the electrons are near the Fermi level and we integrate over a domain of size  $l_m$ . If we assume ergodicity of the wavefunctions,  $\overline{|\psi|^2} = 1/L$  from the normalization condition over the whole volume. Hence

$$|v_{nm}|^2 = \left(\frac{\hbar}{m_e}\right)^2 k_F^2 (\overline{|\psi|^2} l_m)^2 \frac{L}{l_m} = v_F^2 \frac{l_m}{L}. \quad (4.40)$$

From here, we get  $\tilde{G} \sim l_m/L$ , which leads to the Drude result. We will discuss the limited validity of this result in the next subsection.

### 4.2.2 Non-Ergodicity of Wavefunctions

It is clear that Mott's derivation of the Drude formula on the basis of LRT and the random waves conjecture becomes non-applicable if the eigenfunctions are non-ergodic. This is indeed the case for both weak and strong disorder: a typical eigenfunction does not fill the whole accessible phase space. In the ballistic case a typical eigenfunction is not ergodic over the open modes in momentum space, while in the strong localization regime it is not ergodic over the ring in real space [42]. We can demonstrate this point by plotting the participation ratio for various space representations as a function of the disorder strength. Participation ratio is defined as

$$PR \equiv \left[\sum \mathcal{P}^2\right]^{-1}, \quad (4.41)$$

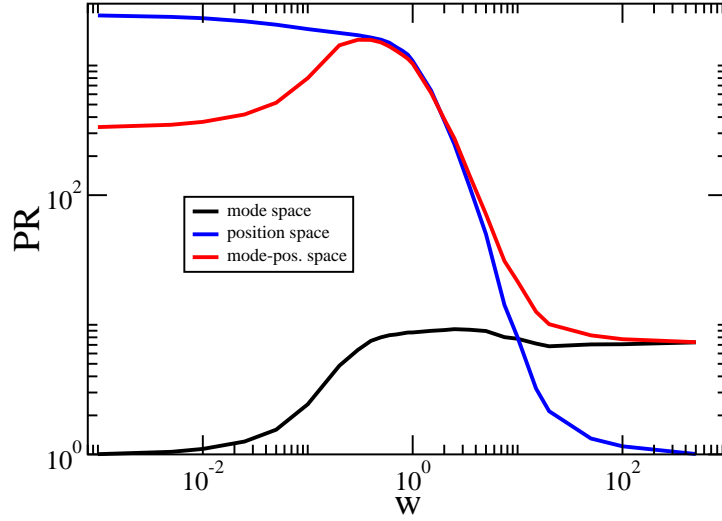


**Figure 4.4:** Participation ratio, defined as  $PR \equiv [\sum \mathcal{P}^2]^{-1}$ , as a characterization of ergodicity, versus disorder  $w$ , in various space representations. Figure from [14].

where  $\mathcal{P}$ , which is the wavefunction density, depends on the space representation. Next we define the coordinates of a site in real space, with  $r_{\parallel}$  for longitudinal direction and  $r_{\perp}$  for transverse direction. In position space  $\mathcal{P}$  is the probability to be at site  $(r_{\parallel}, r_{\perp})$

$$\mathcal{P}_{r_{\parallel}, r_{\perp}} = |\langle r_{\parallel}, r_{\perp} | \Psi \rangle|^2. \quad (4.42)$$

In mode space  $\mathcal{P}$  is the probability to be at mode  $k_{\perp} = m\pi/(M+1)$  where  $m$  integer, and can be written as

$$\mathcal{P}_{k_{\perp}} = \sum_{r_{\parallel}} |\langle r_{\parallel}, k_{\perp} | \Psi \rangle|^2, \quad (4.43)$$

where

$$\langle r_{\parallel}, k_{\perp} | \Psi \rangle = \sum_{r_{\perp}} \langle r_{\parallel}, r_{\perp} | \Psi \rangle \exp(ik_{\perp} r_{\perp}). \quad (4.44)$$

In Fig. 4.4 we see that, as we expected, the participation ratio for mode (momentum) space is smallest in the ballistic regime, and the participation ratio for position space is smallest in the localized regime. This result is in agreement with our intuition: in the ballistic regime due to the lack of scattering events the wavefunction does not spread

over the whole number of accessible modes, while in the localized regime, Anderson localization prevails leading to exponentially localized wavefunction in real space.

We can also describe the overall ergodicity for both spaces using the participation ratio in the hybrid mode-position space where

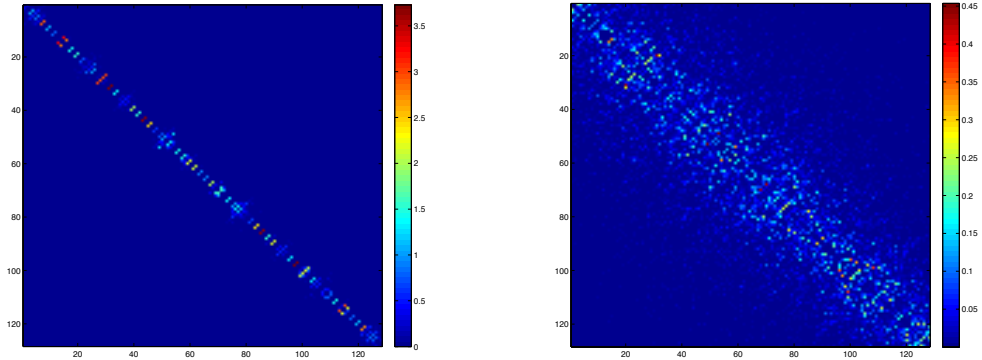
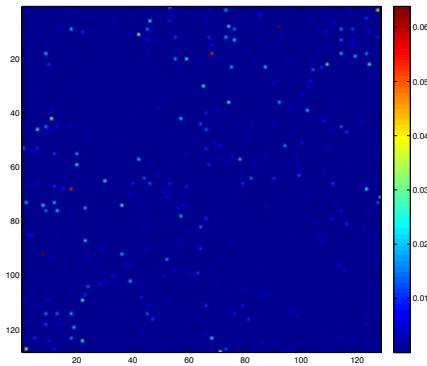
$$\mathcal{P}_{r_{\parallel}, k_{\perp}} = |\langle r_{\parallel}, k_{\perp} | \Psi \rangle|^2. \quad (4.45)$$

From Fig. 4.4 we see that the value of participation ratio in this hybrid space is highest in the diffusive regime. In the ballistic limit, it approximately goes to the number of sites  $L$ , indicating the eigenfunctions are ergodic only in position space but not in mode space. In the localized limit, it approximately goes to the number of modes  $M$ , which means the eigenfunctions are ergodic only in mode space, not in position space.

### 4.2.3 Structural Analysis of the Perturbation Operator

Lack of quantum ergodicity for either weak or strong disorder implies that the perturbation matrix  $v_{nm}$  is very structured and/or sparse [43]. We show this in Fig. 4.5, where in the weak disorder regime the perturbation matrix is structured and sparse, and in strong disorder regime it is very sparse. In the strong disorder case the sparsity is clearer to understand: Eigenstates that are close in energy space are typically distant in real space, and therefore have very small overlap. The large matrix elements comes from the contribution of the eigenstates that reside within the same region in real space, hence the sparsity.

For analytical purposes a better mathematical formulation for this sparsity is required. One can define a sparsity measure  $p$  as the fraction of non-zero elements. A matrix is regarded to be sparse if  $p \ll 1$ . Such a definition assumes a bimodal distribution of matrix elements (Fig. 4.6). For a matrix with a bimodal distribution of elements, sparsity measure  $p$ , and  $X_0$  as the value of all non-zero elements, we can easily calculate the average value of the matrix elements to be  $\langle X \rangle = pX_0$ . However, in general we do

(a) Ballistic regime,  $w = 0.05$ (b) Diffusive regime,  $w = 0.35$ (c) Localized regime,  $w = 7.5$ 

**Figure 4.5:** Perturbation matrix  $|v_{nm}|^2$  for various disorder values  $w$ . Each plot represents a different regime.

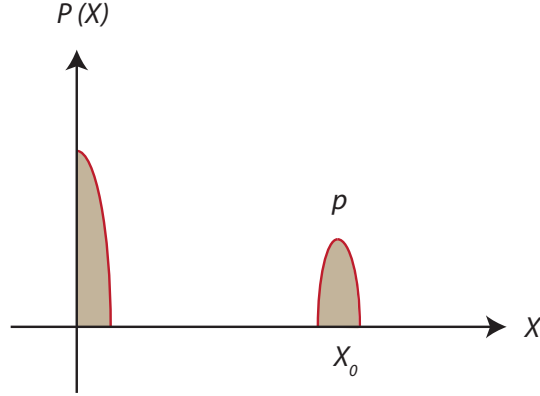


**Figure 4.6:** Bimodal distribution, an idealized distribution function  $P(X)$  for perturbation matrix elements  $X = |v_{nm}|^2$ . In the case of this figure we have  $\langle X \rangle = pX_0$ . Figure from [15].

not find such idealized matrices in nature. After contemplating on this issue, one can conclude that the physically generalized definition of the sparsity measure is  $p \equiv F(\langle X \rangle)$ . Here  $F(X)$  is the probability to find a value larger than  $X$ , which is equivalent to the cumulative distribution of matrix elements of  $\{X\}$ , integrated from above.

### 4.3 Random Matrix Theory Modeling

In this section we introduce a modeling scheme of artificial matrices using RMT that can represent our numerical findings. We need to utilize the appropriate distribution of matrix elements, based on the numerical results. In Fig. 4.7 we plot the cumulative distribution  $F(X)$  for various disorder values from our numerics, and for strong disorder we observe a log-box distribution. In the following subsection we build an analytical reasoning for this type of distribution.

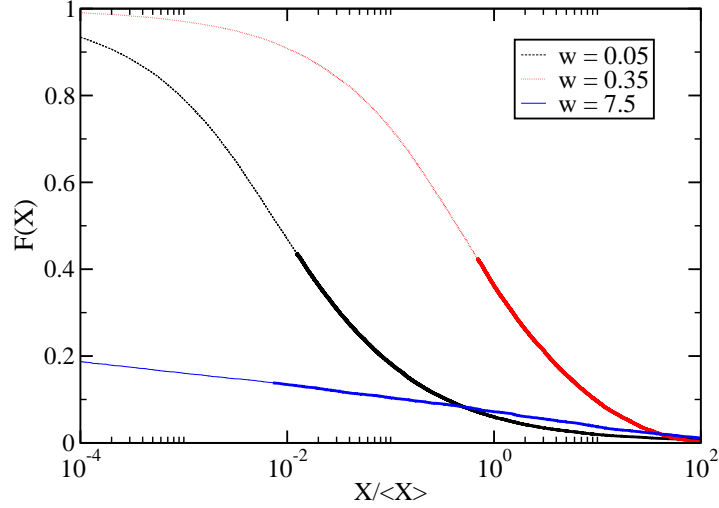


**Figure 4.7:** The cumulative distribution  $F(X)$  of perturbation matrix elements  $X = |v_{nm}|^2$  for disordered quasi-1d ring with various values of disorder. For strong localization one observes a log-box distribution. The non-negligible values, which have  $X > \langle\langle X \rangle\rangle_{\text{SLRT}}$  are indicated by a thicker line. Figure from [14].

### 4.3.1 Log-Box Distribution of Matrix Elements

Given that a generic eigenfunction in the localized regime has an exponential shape  $\psi(r) \approx \exp(-|r - r_0|/l_\infty)$ , we conclude that a typical matrix element of  $|v_{nm}|^2$  has the magnitude

$$X \approx A \exp\left(-\frac{x}{l_\infty}\right) \quad (4.46)$$

where  $x \in [0, L/2]$  has a uniform distribution. Here we define a new variable  $y \equiv x/l_\infty$ , and the above equation becomes

$$X \approx A \exp(-y), \quad (4.47)$$

and  $y \in [y_0 = 0, y_1 = L/(2l_\infty)]$ . Note that in the localized regime  $y_1 \gg 1$ . As  $y$  has a uniform distribution  $P(y)$ , from normalization  $\int_{y_0}^{y_1} P(y) dy = 1$  we have  $P(y) = 1/(y_1 - y_0)$ . We can then find the distribution of  $X$ ,  $P(X)$ , by having  $P(X) dX = P(Y) dy$ , and we obtain

$$P(X) = \frac{1}{X} \frac{1}{y_1 - y_0}, \quad (4.48)$$

where  $X \in [X_1 = A \exp(-y_1), X_0 = A]$ . The mean value of  $X$  is then

$$\begin{aligned} \langle X \rangle &= \int_{X_1}^{X_0} X P(X) dX = \frac{1}{(y_1 - y_0)} \int_{X_1}^{X_0} dX \\ &= \frac{X_0 - X_1}{y_1 - y_0} \approx \frac{2Al_\infty}{L} \end{aligned} \quad (4.49)$$

in the localized regime. The above equation can also be written as

$$\langle X \rangle = \frac{X_0 - X_1}{\ln(X_0) - \ln(X_1)} = \frac{X_0 - X_1}{\ln(X_0/X_1)}. \quad (4.50)$$

The prefactor  $A$  can be determined from the requirement of having  $\tilde{G} \approx l_m/L$ , in agreement with the semiclassical result. By substituting Eq. 4.50 into Eq. 4.18 we have  $A \sim (v_F/M)^2$ .

Using the result for  $P(X)$ , we can then determine the sparsity measure  $p$

$$\begin{aligned} p &= F(\langle X \rangle) = \int_{\langle X \rangle}^{X_0} P(X) dX = \frac{1}{(y_1 - y_0)} \int_{\langle X \rangle}^{X_0} \frac{dX}{X} \\ &= \frac{\ln(X_0) - \ln(\langle X \rangle)}{y_1 - y_0} = \frac{\ln(X_0/\langle X \rangle)}{\ln(X_0/X_1)}. \end{aligned} \quad (4.51)$$

If we substitute Eq. 4.50 into the above equation, the sparsity can be written as

$$p = \frac{\ln\left(\frac{X_0[\ln(X_0/X_1)]}{X_0 - X_1}\right)}{\ln(X_0/X_1)}. \quad (4.52)$$

We define  $\tilde{p} \equiv [\ln(X_1/X_0)]^{-1}$ , and assuming  $X_0 \gg X_1$  we find

$$p \approx -\tilde{p} \ln \tilde{p}. \quad (4.53)$$

By substituting the above equation into Eq. 4.50 (assuming  $X_0 \gg X_1$ ) we obtain  $\langle X \rangle \approx \tilde{p}X_0$ . Hence for a log-box distribution  $\langle X \rangle \sim pX_0$ , as expected from the standard bimodal case.

### 4.3.2 Modeling Results

In Fig. 4.9 we repeat the conductance calculation with artificial matrices given the same sparsity, i.e. log-box distributed elements with the same  $p$  (see Fig. 4.8). We

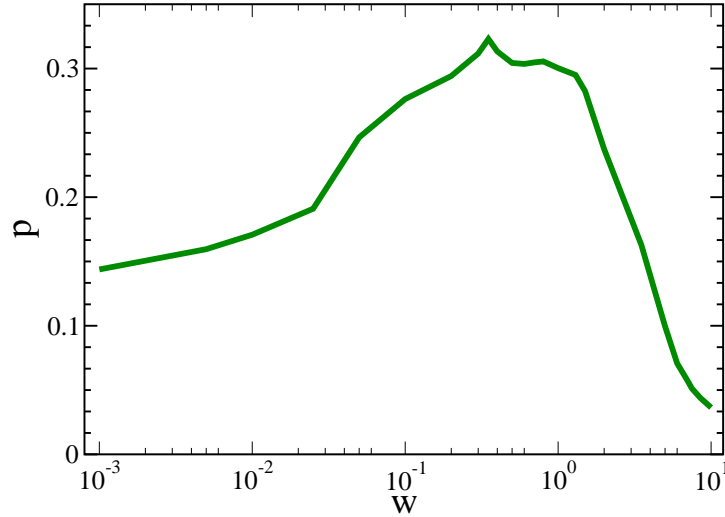


**Figure 4.8:** Matrix sparsity measure  $p$  versus disorder strength  $w$ . A matrix is sparse when  $p \ll 1$ . Figure from [14].

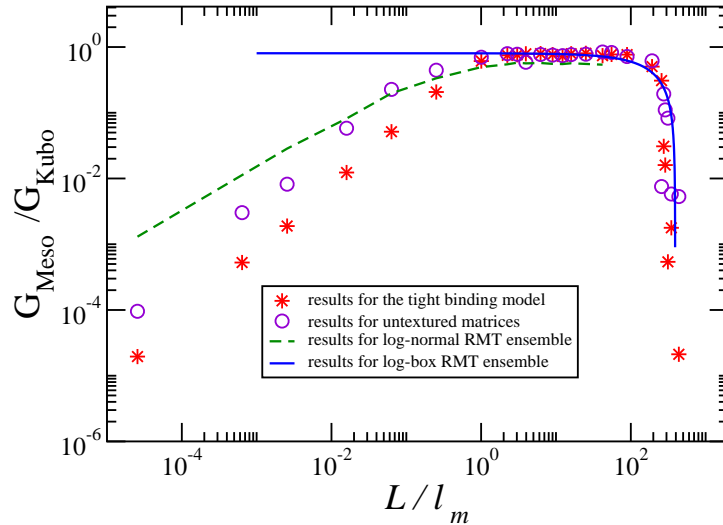


**Figure 4.9:** The ratio  $G_{\text{meso}}/G_{\text{Kubo}}$  versus  $L/l_m = \tilde{G}_{\text{Drude}}^{-1}$ , based on the numerics of Fig. 4.3. We compare with the results from the “untextured” matrices and artificial RMT modeling using sparse matrices with log-normal or log-box distribution of matrix elements. For weak disorder there is only a qualitative agreement, indicating the structure of the perturbation matrix becomes important. Figure from [14].

observe qualitative agreement for strong disorder limit. In the other extreme limit of weak disorder there is no agreement, because we need to use a different distribution of the matrix elements. It turns out that in the ballistic regime  $\log X$  has a wide distribution, but it is not stretched as in the case of a log-box distribution. Rather, it can be modeled as log-normal. Once we use the appropriate distribution we get a reasonable agreement.

### 4.3.3 Generalized Variable Range Hopping Picture

Given a hopping range  $|E_m - E_n| \leq \hbar\omega$  we can look for the typical matrix element  $\bar{X}$  for connected sequences of such transitions, which we find by solving the equation

$$\left(\frac{\hbar\omega}{\Delta}\right) F(\bar{X}) \sim 1. \quad (4.54)$$

For strong disorder, using the value of  $F(X)$  from Eq. 4.51 we have

$$\frac{\ln(X_0/\bar{X})}{\ln(X_0/X_1)} \sim \frac{\Delta}{\hbar\omega}. \quad (4.55)$$

Using the values  $X_0 = (v_F/M)^2$  and  $X_1 = (v_F/M)^2 \exp(-L/2l_\infty)$  from Subsection 4.3.1 we obtain

$$\bar{X} \sim v_F^2 \exp\left(-\frac{\Delta l_\infty}{\hbar\omega}\right), \quad (4.56)$$

where we define  $\Delta_{l_\infty} \equiv (L/l_\infty)\Delta$ , which is the local level spacing between eigenstates localized in the same region. The same procedure can be applied also in the ballistic regime leading to a simpler variation of Eq. 4.56, where the dependence of  $\bar{X}$  on  $\omega$  predominantly reflects the band profile: It follows from the discussion in Subsection 4.1.2 that  $v_{nm}$  is a banded matrix, with a Lorentzian bandprofile whose width  $\sim v_F/l_m$  becomes narrower as disorder is decreased.

The definition of the bandprofile reflects the variation of  $\langle X \rangle$  with  $\omega$ . In complete analogy we define an effective bandprofile that reflects the variation of  $\bar{X}$  with  $\omega$ .

Namely

$$\tilde{C}_{\text{qm-LRT}}(\omega) \equiv 2\pi\rho_F \left(\frac{e}{L}\right)^2 \langle X \rangle \quad (4.57)$$

$$\tilde{C}_{\text{qm-SLRT}}(\omega) \equiv 2\pi\rho_F \left(\frac{e}{L}\right)^2 \bar{X} \quad (4.58)$$

The spectral function in Appendix C is a smeared version of the “bare” spectral function: it is obtained by a convolution  $\tilde{C}_{\text{qm-LRT}}(\omega) * \delta_{\gamma_{\text{brd}}}(\omega)$ . More generally we argue that the generalized version of Eq.4.16 is

$$G = \frac{1}{2} \left(\frac{e}{L}\right)^2 \rho_F \int \tilde{C}_{\text{qm}}(\omega) \delta_{\gamma_{\text{brd}}}(\omega) d\omega \quad (4.59)$$

where the appropriate LRT/SLRT spectral function should be used. This way of writing allows one to obtain an approximation for the mesoscopic conductance using a Kubo-like calculation. In particular for strong disorder we get an integral over  $\exp(-\hbar|\omega|/\gamma_{\text{brd}}) \exp(-\Delta_{l_\infty}/\hbar|\omega|)$ , as expected from the VRH phenomenology. In the weak disorder regime the VRH integral is not the same because a log-normal rather than log-box distribution is involved. We have verified that the generalized VRH integral gives a qualitative approximation to the actual resistor network calculation.

## 4.4 Summary

Within the framework of SLRT we use the assumption that the transitions between levels are given by Fermi Golden Rule, but the energy absorption rate is determined using a resistor network picture. The calculation method used is similar to the method used in solving a percolation problem, but the percolation is in energy space rather than real space. The calculation generalizes the variable range hopping picture and treats equivalently the weak and strong disorder regimes. Appropriate distribution for the elements of the perturbation matrix (either log-box or log-normal) should be assumed within the RMT framework.

A recent study [44] has attempted to go beyond the FGR approximation. If its results could be extended beyond the diffusive regime, it is possible to extend SLRT into the non-linear regime.

A few words are in order regarding the implicit role of the environmentally induced relaxation process that determines the steady state of the system. Within SLRT one assumes that the FGR rate of the driven transitions ( $\Gamma_{\text{FGR}} \propto \varepsilon^2 g_{nm}$ ) is large compared to the relaxation rate  $\gamma_{\text{rlx}}$ . The inelastic relaxation effect can be incorporated into the SLRT framework by considering a non-symmetric  $g_{nm}$  as implied, perhaps by detailed balance considerations. If the relaxation process is the predominant effect ( $\Gamma_{\text{FGR}} < \gamma_{\text{rlx}}$ ) then we are back in the LRT regime [45] where the Kubo-Drude result applies [9]. If the mean free path becomes smaller than the length of the ring, then the scaled conductance  $\tilde{G}$  is simply identified as the average transmission per channel as in the theory of Landauer [46].

## Chapter 5

# SLRT for Systems at Metal-Insulator Transition: Preliminary Results

In this chapter, we apply SLRT to the Harper model. This is a prototype solid-state model which allows us to discuss the Metal-Insulator transition in one-dimension, thus bypassing the numerical deficiencies appearing in higher-dimensional systems due to memory restrictions. Although this is a work in progress [16], we feel that it makes sense for the completeness of this Thesis to include this chapter. In section 5.1 we introduce the model, then discuss the idea of criticality in the model. Section 5.2 presents the results for conductance based on the Landauer approach. In section 5.3 we present the numerical results of SLRT conductance for a Harper ring model and compare them with the results of the Drude and Kubo formalisms. Section 5.4 deals with the fractal structures of the eigenstates and how it affects the structures of the perturbation matrix. We end this chapter by summarizing our findings thus far.

## 5.1 Harper Model and Criticality

The on-site potential that characterizes the Harper model has the form  $\epsilon_n = 2\lambda \cos(2\pi\sigma n + \theta)$ , where  $\theta$  is a random phase that will allow us later on to perform statistical averaging. The tight-binding equation becomes

$$V(c_{n+1} + c_{n-1}) + \lambda \cos(2\pi\sigma n + \theta) c_n = E c_n. \quad (5.1)$$

This type of model was first studied by Harper [47]. If  $\sigma$  is an irrational number, the periodicity of the potential ( $\sigma^{-1}$ ) is irrational with respect to the periodicity of the lattice (hence it is “quasiperiodic”). In this respect, the Harper model shows properties between those of a periodic and a random potential.

To identify the value of  $\lambda$  for which the phase transition takes place in the Harper model, we will follow the method of [48, 49]. We consider a Harper model with infinite sites and irrational  $\sigma$ . We want to write the simultaneous equations of Eq. 5.1 in reciprocal lattice representation. If  $f_m$  is the projection of the wavefunction at  $m$ -th reciprocal lattice site, we can relate  $c_n$ 's and  $f_m$ 's using the following transformation

$$c_n = \exp(in\alpha) \sum_{m=-\infty}^{+\infty} \exp[im(2\pi\sigma n + \theta)] f_m, \quad (5.2)$$

where  $\alpha$  is a phase. Applying this to Eq. 5.1, and then grouping the terms which have the same exponential terms, results in the following equation in the reciprocal lattice space

$$\frac{\lambda}{2}(f_{m-1} + f_{m+1}) + 2V \cos(2\pi\sigma m + \alpha) = E f_m. \quad (5.3)$$

If  $\lambda = 2V$ , Eq. 5.3 has the same form as Eq. 5.1. If the eigenstates are localized (and hence normalizable) in reciprocal space, the sum  $\sum_m |f_m|^2$  is finite. Based on this result, Eq. 5.2 has a converging sum term, and satisfies Bloch's theorem. Hence the eigenstates are extended in real space, which is the metal state. Using a symmetry condition between Eq. 5.1 and Eq. 5.3, we can also show that when the eigenstates are localized in real space (insulator state), they are extended in reciprocal space.

When the eigenstates are localized, we can write an expression of the localization length using the Thouless relation of Subsection 2.3.2. In real space the inverse localization length is given by

$$l_1^{-1}(E) = \int dE' \ln \left| \frac{E - E'}{V} \right| \rho(E'), \quad (5.4)$$

and in reciprocal space it is

$$l_2^{-1}(E) = \int dE' \ln \left| \frac{2(E - E')}{\lambda} \right| \rho(E'). \quad (5.5)$$

The two localization lengths are related by

$$l_1^{-1}(E) = l_2^{-1}(E) + \ln(\lambda/2V). \quad (5.6)$$

When the eigenstates are localized, the localization length has to be a positive number. Using the condition obtained in the previous paragraph, when the eigenstates are localized in real space, they are extended in reciprocal space ( $l_2(E) \rightarrow \infty$ ) and

$$l_1^{-1}(E) = \ln(\lambda/2V) > 0, \quad (5.7)$$

which means  $\lambda > 2V$ . Conversely, if the eigenstates are extended in real space ( $l_1(E) \rightarrow \infty$ ), they are localized in reciprocal space and

$$l_2^{-1}(E) = \ln(2V/\lambda) > 0, \quad (5.8)$$

which means  $\lambda < 2V$ . We thus conclude that the transition between localized and extended states occurs when  $\lambda = 2V$ . At this point, the wavefunction possesses a fractal structure.

The fractal nature of the wavefunctions can be shown using a phase space representation. Due to Heisenberg's uncertainty principle, it is hard to define phase space of a quantum state where we have perfect localization in position or momentum space [50]. One way to represent the phase space of a quantum state with a wavefunction  $\psi(x)$  is by using the Husimi function [51], which is a Gaussian smearing of the Wigner function

$$W(x, k) = \int dy \exp(iky) \psi^* \left( x + \frac{y}{2} \right) \psi \left( x - \frac{y}{2} \right), \quad (5.9)$$

where  $k$  is the wave number. The Husimi function itself can be written as

$$\varrho(x, k) = \frac{1}{\pi} \int dx' dk' \exp \left[ -\frac{(x-x')^2}{2\sigma_\varrho^2} - 2\sigma_\varrho^2(k-k')^2 \right] W(x', k'), \quad (5.10)$$

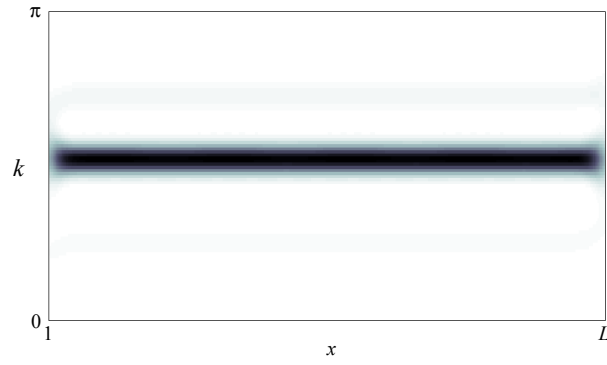
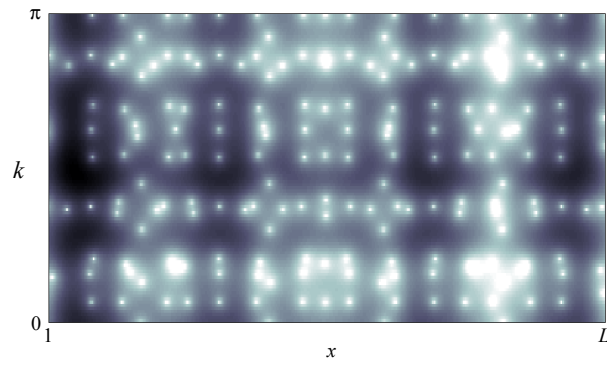
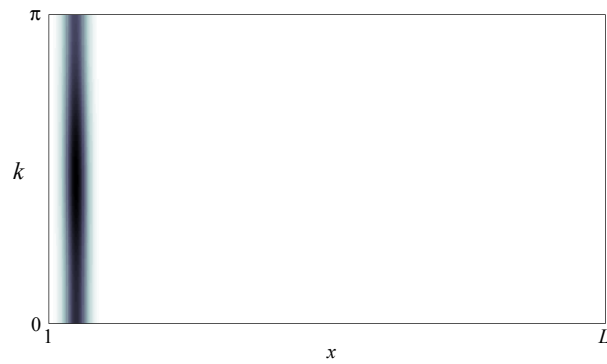
where  $\sigma_\varrho$  is the smearing width of the Husimi function. By substituting Eq. 5.9 to Eq. 5.10, we obtain

$$\varrho(x, k) = \left| \int dx' \psi(x') \frac{1}{(2\pi\sigma_\varrho)^{1/4}} \exp \left[ -\frac{(x-x')^2}{4\sigma_\varrho^2} - ikx' \right] \right|^2. \quad (5.11)$$

$\sigma_\varrho$  is essentially a free parameter, but in our calculations we adopt the suggestion of [50]: an equal relative uncertainty in position and momentum space ( $\Delta x/L = \Delta k/2\pi$ ), and minimal uncertainty based on Heisenberg's uncertainty principle ( $\Delta x \Delta k = 1/2$ ). Using these two conditions we have  $\sigma_\varrho = \Delta x = \sqrt{L/4\pi}$ .

In Fig. 5.1 we plot the Husimi function for the Harper model with size  $L = 377$  and  $\sigma = (\sqrt{5} - 1)/2$  for an eigenstate near the band center. Since we have a discrete lattice, so the integral in Eq. 5.11 becomes a sum over  $x'$ , and we discretize the momentum space as well. As the Husimi function is symmetric,  $\varrho(x, -k) = \varrho(x, k)$ , it is enough to plot only the upper half of the phase space where  $k \in [0, \pi]$ . In the extended regime, the Husimi function is localized in momentum space and extended in position space (see Fig. 5.1(a)). In the localized regime the Husimi function is localized in position space and extended in momentum space (see Fig. 5.1(c)). These results agree with the expectation of the structures of the wavefunctions from above. Meanwhile at the critical point, a large part of the phase space is filled, suggesting a fractal behavior at the critical point (see Fig. 5.1(b)).

In fact, not only the eigenstates of the Harper model are fractal, but also its spectrum shows fractal properties. Specifically for  $\sigma$  irrational, the energy spectrum is a Cantor set. In Fig. 5.2 we report the energy spectrum as a function of  $\sigma$ , the emerging structure is known as the Hofstadter butterfly [52].

(a) Extended regime,  $\lambda = 0.5$ (b) Critical point,  $\lambda = 2$ (c) Localized regime,  $\lambda = 8$ 

**Figure 5.1:** Husimi functions for the Harper model with various values of potential strength  $\lambda$ , for an eigenstate that is close to the band center and  $L = 377$ . Due to the symmetry of the Husimi function  $\varrho(x, -k) = \varrho(x, k)$ , it is enough to plot only the upper half of the phase space.

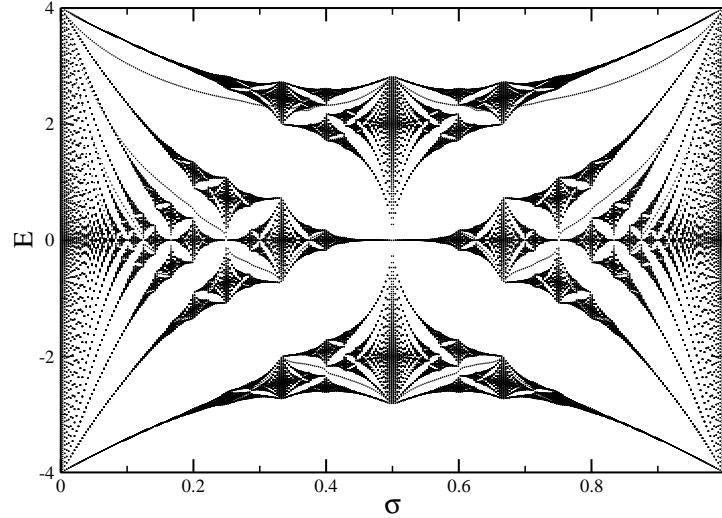


**Figure 5.2:** Plot of the energy spectrum versus  $\sigma$  for the Harper model, more commonly known as Hofstadter butterfly. This plot shows fractal structure in the energy spectrum of the Harper model.

## 5.2 Landauer Picture at Critical Point

As shown in the previous chapter, in Landauer picture, the scaled conductance  $\tilde{G} = G(2\pi\hbar/e^2M)$  equals the average transmission  $T$  of the lattice. In the case of Harper model with irrational  $\sigma$  and at critical point ( $\lambda = 2V$ ), Ref. [53] has calculated the dependence of  $T$  on system size  $L$  using the transfer matrix method (see Subsection 2.1.2). The study found that  $T$  approximately follows a power law

$$T(L) \propto L^{-\gamma}, \quad (5.12)$$

where the value of the exponent  $\gamma$  depends on  $\sigma$ , specifically its degree of irrationality. We call this behavior the “generalized Ohm’s law.” In Fig. 5.3 we redo the calculation for various values of  $\sigma$ . An ensemble average of the logarithm of transmission  $\langle \ln T \rangle$  is calculated by generating realizations of the Harper potential with a phase  $\theta$  given by a uniform distribution. For  $\sigma$  the inverse of the *golden ratio*  $(\sqrt{5} - 1)/2$  (red line in Fig. 5.3), we have  $\gamma \approx 1.0$ , and hence the Landauer conductance has a standard Ohmic behavior ( $G \propto 1/L$ ).

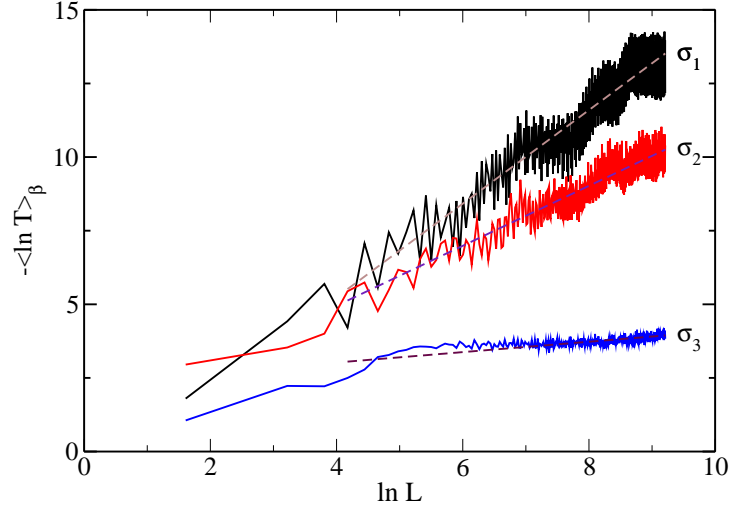


**Figure 5.3:** Natural logarithm of transmission coefficient  $T$  versus natural logarithm of system size  $L$  for the Harper model with energy  $E = 0$  and various values of  $\sigma$ :  $\sigma_1 = (\sqrt{2} - 1)$ , where  $\gamma >$  (black line);  $\sigma_2 = (\sqrt{5} - 1)/2$ , where  $\gamma \approx 1$  (red line); and  $\sigma_3 = (\pi - 3)$ , where  $\gamma < 1$  (blue line). The dashed lines indicate the best linear fit of the data.

Here we used an averaging of  $\langle \ln T \rangle_\theta$  instead of  $\langle T \rangle_\theta$  as it was shown that the distribution of  $T$  is approximately log-normal, and logarithmic averaging is useful in reducing the large fluctuations of  $T$  [53]. It was also found that logarithmic averaging over various values of energy  $E$  gives approximately the same result as averaging over different realizations of  $\theta$ , provided  $E$  is far from the edges of the energy spectrum [53].

### 5.3 Application of SLRT: Numerical Results

For Harper ring model with  $\sigma = (\sqrt{5} - 1)/2$  and  $V = 1$ , the plots of scaled conductances  $\tilde{G}_{\text{Drude}}$ ,  $\tilde{G}_{\text{Kubo}}$ , and SLRT  $\tilde{G}_{\text{meso}}$  as a function of potential strength  $\lambda$  are shown in Fig. 5.4. At first observation it seems that the behavior of the SLRT conductance and Kubo conductance are quite similar to the corresponding quasi-1d conductances: SLRT conductance results approaches Kubo results near the critical point, while in the extended and localized regimes, there is a departure of the SLRT results from the Kubo

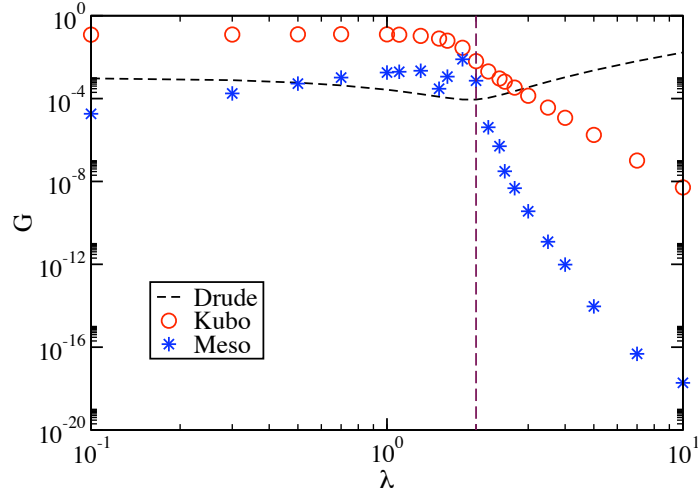


**Figure 5.4:** Scaled conductances  $\tilde{G}_{\text{Drude}}$ ,  $\tilde{G}_{\text{Kubo}}$ , and  $\tilde{G}_{\text{meso}}$  versus potential strength  $\lambda$  for the Harper ring model with  $L = 1000$  and  $\sigma = (\sqrt{5} - 1)/2$  and  $V = 1$ . The dashed vertical line is the critical point  $\lambda = 2$ .

results. To explain the departure, we might be able to use the ergodicity argument that was used in Chapter 4 as well.

We need to study more carefully the properties of the SLRT conductance at the critical point  $\lambda = 2$ , and in the following we will focus on its scaling properties with respect to the system size. The results of  $\tilde{G}_{\text{meso}}$  are reported in Fig. 5.5 together with the corresponding data for the  $\tilde{G}_{\text{Drude}}$  and  $\tilde{G}_{\text{Kubo}}$  for various system sizes  $L$ . It turns out that the SLRT conductance has a different scaling behavior when compared to the scaling behaviors of Drude and Kubo conductances. From the figure it is clear that both  $\tilde{G}_{\text{Drude}}$  and  $\tilde{G}_{\text{Kubo}}$  follow Ohmic behavior  $\gamma = 1.0$ , in contrast to the SLRT  $\tilde{G}_{\text{meso}}$  for which we found that the best linear fit gives a power law exponent  $\gamma \approx 1.7$ . Thus  $\tilde{G}_{\text{meso}}(L) < \tilde{G}_{\text{Kubo}}(L)$ . Although this finding is in line with our expectations that  $G_{\text{meso}}$  captures the long time dissipation rate which is dictated by bottlenecks in the energy flow due to sparsity in the current matrix, a better numerical analysis is needed in order to conclude on the power law behaviour of  $\tilde{G}_{\text{meso}}$ .

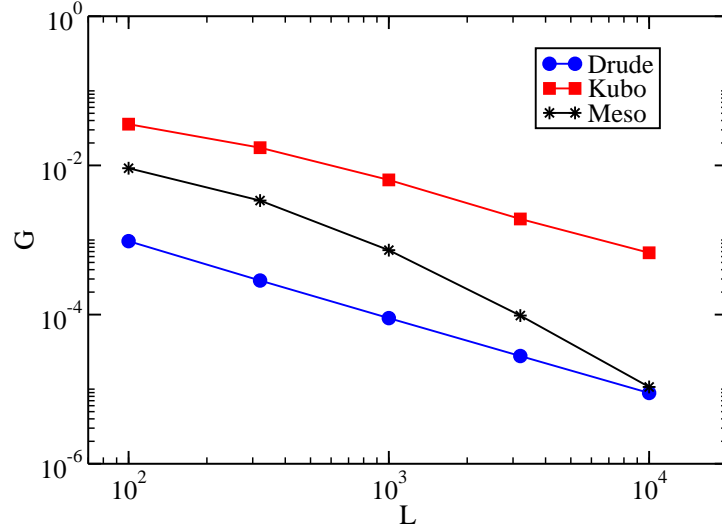


**Figure 5.5:** Scaled conductances  $\tilde{G}_{\text{Drude}}$ ,  $\tilde{G}_{\text{Kubo}}$ , and  $\tilde{G}_{\text{meso}}$  versus ring circumference  $L$  for the Harper ring model with  $\sigma = (\sqrt{5} - 1)/2$  at the critical point.

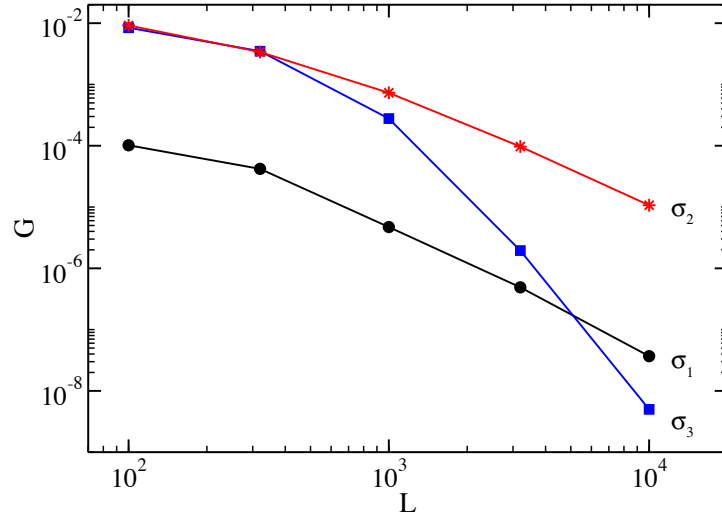


**Figure 5.6:** Scaled mesoscopic conductance  $\tilde{G}_{\text{meso}}$  versus ring circumference  $L$  for the Harper ring model for various values of  $\sigma$ . The  $\sigma$  values and the color coding are the same as in Fig. 5.3:  $\sigma_1 = (\sqrt{2} - 1)$  (black line);  $\sigma_2 = (\sqrt{5} - 1)/2$  (red line); and  $\sigma_3 = (\pi - 3)$  (blue line).

If we vary the value of  $\sigma$ , we find that both Drude and Kubo conductances still follow Ohmic behavior. In fact, this is to be expected for the semiclassical Drude results. Meanwhile, for mesoscopic conductance, as shown in Fig. 5.6, the value of  $\gamma$  depends on  $\sigma$ , but the dependence is different than  $\sigma$  dependence of Landauer conductance in the previous section. This latter discrepancy is not surprising as the two quantities describe different physical set-ups. We remind again that the Landauer conductance is dealing with the transmission coefficient as it discuss the conductance of a sample coupled with leads, while the SLRT analyzes the properties of an “absorption coefficient” due to noisy driving. In fact, the different  $\gamma$  values that we are observing for various irrational  $\sigma$ 's are directly related with the developed structures in the current matrix. For example, more/less sparsity is determined by the level of fractality of the wavefunctions and affects the transport since it will introduce more/less bottlenecks in the energy flow.

Naturally, as in the case of quasi-1d rings, we are interested to build an analytical model that can explain the numerical results. The large discrepancy of the SLRT and LRT results, at least at first glance, can be attributed to the structure and/or sparsity of the perturbation matrix. We will expand this idea in the next section, where we try to relate the structures of the perturbation matrix with the fractal properties of the system at criticality.

## 5.4 Fractal Structures of Perturbation Matrix

As we discussed previously, at the critical point, the eigenstates and the spectrum possess fractal structures. We find that fractal structures are manifested in the perturbation matrix as well. Fig. 5.7 shows this by displaying various cuts of the perturbation matrix  $|v_{nm}|^2$ , where each consecutive matrix is a submatrix of the previous one. One can see that the matrices possess similar structures, limited only by the discreteness of the energy spectrum, which comes from the finite size of the ring.

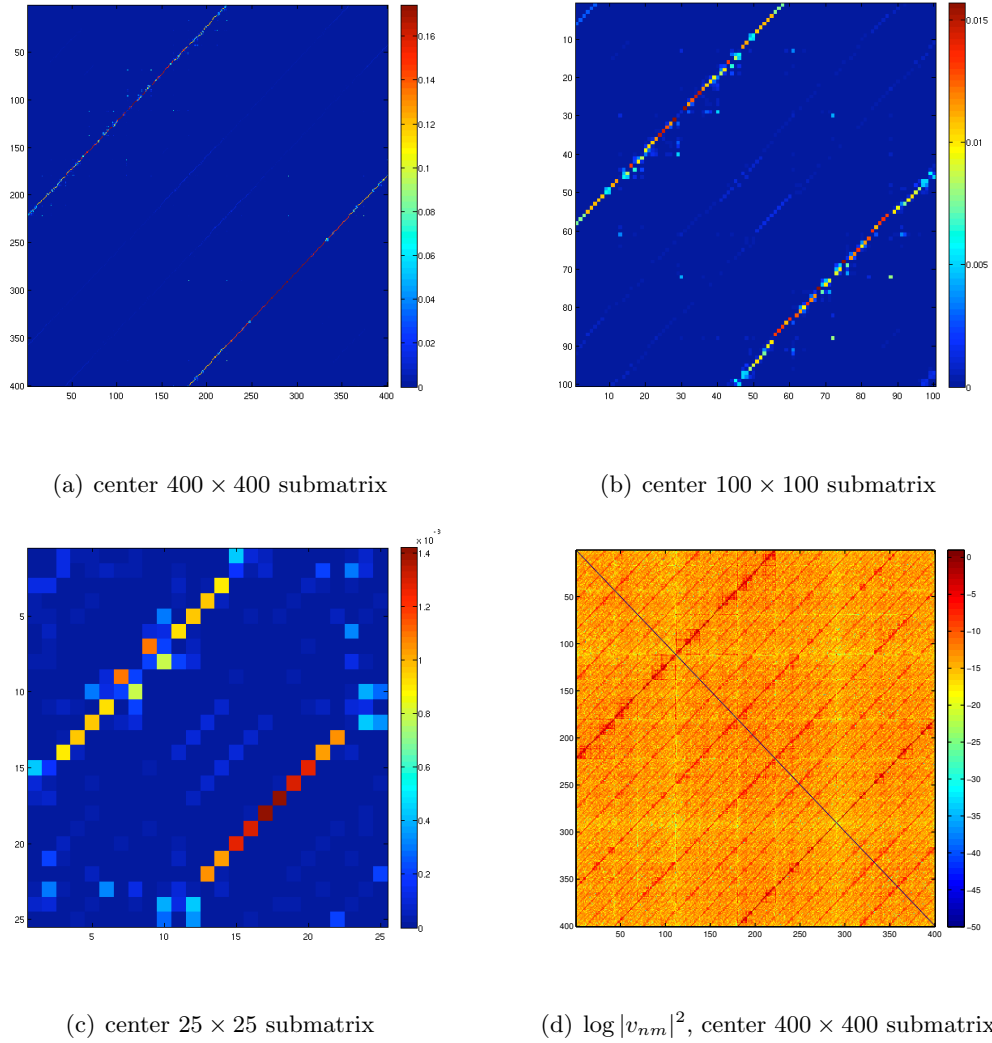


**Figure 5.7:** Different cuts of the perturbation matrix  $|v_{nm}|^2$  for the Harper ring model with  $L = 3200$  and  $\sigma = (\sqrt{5} - 1)/2$ , displaying self-similar structures. In (d) we take the natural logarithm of the matrix elements of (a) to emphasize the structures of the matrix.

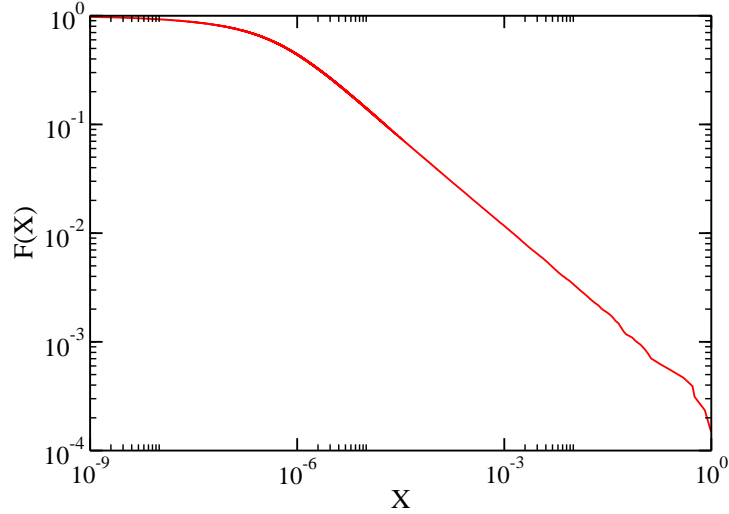


**Figure 5.8:** Cumulative distribution  $F(X)$  of perturbation matrix elements  $X = |v_{nm}|^2$  for the Harper model with  $L = 3200$  and  $\sigma = (\sqrt{5} - 1)/2$ . The tails of  $F(X)$  follows power law  $F(X) \approx X^{-\alpha}$  where  $\alpha \approx 0.54$ .

To analyze the fractal structure of the perturbation matrix further, in Fig. 5.8 we plot the cumulative distribution of matrix elements  $F(X)$  for  $\sigma = (\sqrt{5} - 1)/2$ , and we find that the tail of the distribution follows a power law  $F(X) \approx X^{-\alpha}$ , with a best fit giving the power law exponent  $\alpha \approx 0.54$ . In fact, we can relate  $\alpha$  and the fractal dimensions of Harper model. We define the ratio

$$\beta \equiv \frac{D_2^\mu}{D_2^\psi}, \quad (5.13)$$

where  $D_2^\mu$  is the correlation dimension of the spectrum and  $D_2^\psi$  is the correlation dimension of the eigenfunctions. As shown in previous chapters, the Fermi Golden Rule (FGR) transition rates,  $\Gamma$ , are proportional to the perturbation matrix elements  $|v_{nm}|^2 = X$ .  $\Gamma$  is, by definition, the inverse of the lifetime  $t_l$  of an initially excited state. For a fractal system, the spreading of the variance of a wavepacket follows the relation  $(\Delta x)^2 \sim t^{2\beta}$  [54], and hence

$$\Delta x \sim t^\beta \sim \frac{1}{\Gamma^\beta}. \quad (5.14)$$

Furthermore, the spreading  $\Delta x$  at  $t = t^*$  corresponds to the number of states  $N$  that

are affected by the excitation up to  $t^*$ , assuming an initial excitation at  $t = 0$ . These states are the states that have lifetimes  $t_l < t^*$ , or  $\Gamma > \Gamma^* = 1/t^*$ .  $\Delta x$  can then be written as the expression

$$\Delta x \sim N(\Gamma^*) \sim \int_{\Gamma^*}^{\infty} P(\Gamma) d\Gamma \quad (5.15)$$

where  $P(\Gamma)$  is the distribution of  $\Gamma$ . As  $\Gamma \sim X$ , the integral on the above equation is just the cumulative distribution of matrix elements  $F(X)$ , and the whole expression can be rewritten as

$$F(X) \sim X^{-\beta}. \quad (5.16)$$

Using this result we calculated  $\beta = \alpha \approx 0.54$ . This result is relatively close to the value of  $\beta$  calculated using other methods [54], which found  $\beta \approx 0.46$ . Based on this result, we conclude that the self-similar structures of the perturbation matrix are indeed caused by the fractal structures of the eigenfunctions and of the energy spectra.

## 5.5 Summary

For the Harper ring model, the mesoscopic conductance that is calculated using SLRT has a large discrepancy with Kubo-Drude and Landauer results. We conjecture that this is a result of the scale-free behavior of systems at a phase transition. We show that the perturbation matrix actually possesses a self-similar structure, which can be traced back to the fractal behaviour of the eigenstates and eigenvalues of the system. The heuristic picture that we have in mind is as follows: The diffusion in energy space takes place now in a fractal structure dictated by the current operator  $I$  (see Fig. 5.7). Thus, the energy diffusion is anomalous resulting in a super-ohmic conductance law.

We hope that this work will pave the way to understand the behavior of the absorption coefficient at Metal-Insulator transition. This theoretical understanding will find applications not only for the analysis of the Harper model but also to quantum Hall and high dimensional disorder systems at the critical point.

## Chapter 6

# Summary and Perspectives

In this Thesis we applied semi-linear response theory (SLRT) to determine the conductance within two types of mesoscopic ring systems: the disordered quasi-1d ring and Harper model.

For disordered quasi-1d rings, we studied the dependence of conductance on the disorder strength. We showed that while in the diffusive regime SLRT agrees with linear response theory (LRT/Kubo) and semiclassical (Drude) approximations, in the ballistic and localized regimes there are discrepancies between SLRT results and Drude-Kubo results. We argued that these discrepancies come from the sparsity of the perturbation matrix. The latter is associated with the fact that the wavefunctions in these two regimes lose ergodicity (in mode and position space respectively). We then introduced a random matrix theory (RMT) model based on the analysis of the statistical properties of the current operator matrix elements, and proposed a generalization of the variable range hopping (VRH) approach in order to estimate the conductance. We have discussed the applicability of these models by comparing them with the numerical results. Both approximations showed qualitative agreement with SLRT, provided we used the appropriate distribution of matrix elements in the appropriate regimes: log-normal for weak disorder, and log-box for strong disorder.

For the Harper model, we studied the dependence of conductance to system size at the critical point. We have found that the mesoscopic conductance scales in a power law manner, albeit with a different exponent from the one given by the Drude-Kubo and Landauer approaches. Still, much more work is needed to understand the origin of these discrepancies and connect them to the critical structures of the eigenfunctions and eigenvalues. We also found that the perturbation matrix exhibits fractal structures at the critical point. A qualitative argument allowed us to connect the distribution of the matrix elements of the current operator with the fractal dimensions of the spectrum and eigenstates of the Harper model.

There are numerous ways to extend these studies, both within and beyond the framework of the two ring systems. For our quasi-1d studies, we focused on disorder strength dependence of the conductance. This allowed us to identify the similarities and differences between the SLRT and the Kubo-Greenwood results. Currently, we extend our studies [15] to understanding the scaling properties of mesoscopic conductance with respect to both the system size and localization length. The distribution of mesoscopic conductance and the analysis of its fluctuations is another promising direction. This will shed light on the question: How is the so-called *Universal Conductance Fluctuations* (UCF) reflected in the frame of SLRT? For both systems, it may be interesting to see how the level broadening, which can be due to noisy driving or interaction with the environment, affects the conductance results. We can also apply SLRT to other systems exhibiting Metal-Insulator transition, i.e. disordered 2d systems in the presence of magnetic field and 3D lattices at critical disorder strength. The aim will be to build a theory that can explain SLRT results in critical systems in general.

Semi-linear response theory is a novel framework to study the conductance of mesoscopic objects. It goes beyond the traditional LRT/Kubo framework, and describes equivalently a wide range of regimes. Application of SLRT to mesoscopic systems can reveal new insights about their transport properties.

## Appendix A

# Kramers-Kronig Relation

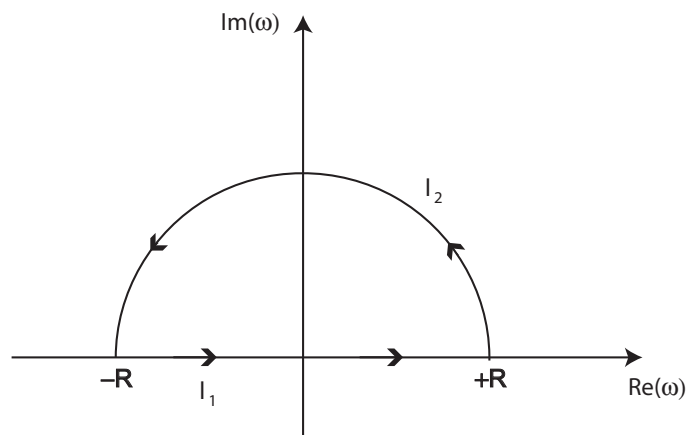


**Figure A.1:** The path of the integration of Eq. A.1

We consider  $\sigma(\omega)$  an analytic function on the complex plane. The integration

$$\oint \frac{d\omega}{2\pi} \sigma(\omega) \exp(-i\omega\tau) = 0 \quad (\text{A.1})$$

along a semicircular loop of radius  $R \rightarrow \infty$  as shown in Fig. A.1, with  $\tau < 0$ , can be

broken down into

$$\lim_{R \rightarrow \infty} \int_{-R}^{+R} \frac{d\omega}{2\pi} \sigma(\omega) \exp(-i\omega\tau) + \lim_{R \rightarrow \infty} \int_{l_2} \frac{d\omega}{2\pi} \sigma(\omega) \exp(-i\omega\tau) = 0, \quad (\text{A.2})$$

where  $l_2$  is the semicircular path from  $+R$  to  $-R$  along the upper half of the complex plane. We will make use of Jordan's Lemma which states that if a function  $f(\omega)$  is analytic on the upper half of the complex plane and  $f(z) \rightarrow 0$  as  $|z| \rightarrow \infty$ , then for every positive  $a$ ,

$$\lim_{R \rightarrow \infty} \int_{l_2} f(z) \exp(iaz) dz = 0, \quad (\text{A.3})$$

if we integrate along a semicircular arc on the upper half of the complex plane with radius  $R$  as shown by  $l_2$  in Fig. A.1 [55]. Applying this lemma to Eq. A.2 results in the second integration term equals zero. The remaining term is the Fourier transform of the function  $\sigma(\omega)$ , which is

$$\sigma(\tau) = \lim_{R \rightarrow \infty} \int_{-R}^{+R} \frac{d\omega}{2\pi} \sigma(\omega) \exp(-i\omega\tau) = 0, \quad (\text{A.4})$$

for  $\tau < 0$ . Eq. A.4 can also be seen as the result of the ‘‘causality principle’’, as the effect cannot precede the cause (which happens here at  $\tau = 0$ ).

Now we consider an integral

$$\oint \frac{dz}{2\pi i} \frac{\sigma(z)}{z - \omega} \quad (\text{A.5})$$

along the same semicircular loop with  $R \rightarrow \infty$  as in Fig. A.1, where here  $\omega$  is a complex number. According to Cauchy's integral formula [55], for a function  $g(z)$  analytic on and inside the domain of integration,

$$\oint \frac{dz}{2\pi i} \frac{g(z)}{z - z_0} = \begin{cases} 0 & \text{if } z_0 \text{ is outside the domain of integration} \\ g(z_0) & \text{if } z_0 \text{ is inside the domain of integration.} \end{cases} \quad (\text{A.6})$$

Applying this to Eq. A.5, where  $z = \omega' + is$  where  $\omega'$  is a real number and  $s$  is a positive number with  $s \rightarrow 0^+$

$$\oint \frac{d\omega'}{2\pi i} \frac{\sigma(\omega' + is)}{[\omega' - (\omega - is)]} = 0, \quad (\text{A.7})$$

since  $\omega' - is$  is on the lower half of the complex plane. Again, the integration can be broken down as in Eq. A.2 to be an integration over the line along the real axis  $l_1$  and along the semicircular arc  $l_2$ . Using Jordan's lemma, the integration along  $l_2$  is again zero. This gives

$$\lim_{s \rightarrow 0^+} \int_{-\infty}^{+\infty} \frac{d\omega'}{2\pi i} \frac{\sigma(\omega' + is)}{[\omega' - (\omega - is)]} = 0. \quad (\text{A.8})$$

Now we will use the principal value identity [56] to Eq. A.8, in which for a real number  $x$

$$\lim_{s \rightarrow 0^+} \frac{1}{x \pm is} = \mp i\pi\delta(x) + PV \frac{1}{x} \quad (\text{A.9})$$

where we have used the definition of Cauchy's principal value [55]

$$PV \int_{-\infty}^{+\infty} f(x) dx \equiv \lim_{R \rightarrow \infty} \int_{-R}^{+R} f(x) dx. \quad (\text{A.10})$$

This results in

$$\sigma(\omega) = -PV \int_{-\infty}^{+\infty} i \frac{d\omega'}{\pi} \frac{\sigma(\omega')}{(\omega' - \omega)}. \quad (\text{A.11})$$

The function  $\sigma(\omega')$  is a complex function, and we can decompose it to its real and imaginary components:  $\sigma(\omega') = \sigma_1(\omega') + i\sigma_2(\omega')$ . If we equate the real parts and the imaginary parts of Eq. A.11 we obtain the Kramers-Kronig relation

$$\sigma_1(\omega) = PV \int_{-\infty}^{+\infty} \frac{d\omega'}{\pi} \frac{\sigma_2(\omega')}{(\omega' - \omega)} \quad (\text{A.12})$$

$$\sigma_2(\omega) = -PV \int_{-\infty}^{+\infty} \frac{d\omega'}{\pi} \frac{\sigma_1(\omega')}{(\omega' - \omega)}. \quad (\text{A.13})$$

## Appendix B

# Fluctuation-Diffusion Relation

There is a simple linear response (Kubo) expression that relates the diffusion coefficient to the power spectrum  $\tilde{C}(\omega)$  of the fluctuations of the acting force. Although the results can be stated for a general external force acting on our system, in the following we will assume one of the traditional mesoscopic set-ups: Namely, we can write the generalized force, in this case being the average current  $I$  through the ring

$$\mathcal{F} = -\frac{\partial \mathcal{H}}{\partial \Phi} = \frac{ev}{L}, \quad (\text{B.1})$$

Assuming a steady state current, the time derivative of  $\mathcal{H}$  can be written as

$$\frac{d\mathcal{H}}{dt} = -\dot{\Phi}I, \quad (\text{B.2})$$

which can be integrated to give us

$$\mathcal{H}(t) - \mathcal{H}(0) = -\int_0^t \dot{\Phi}(t')I(t')dt' \approx -\dot{\Phi} \int_0^t I(t')dt'. \quad (\text{B.3})$$

In the second equality we assumed that the rate of change of the magnetic flux is very small (DC limit) and thus  $\dot{\Phi}$  is constant.

We write the energy dispersion, averaged over a microcanonical ensemble, as

$$\begin{aligned} (\Delta E)^2 &= \langle (\mathcal{H}(t) - \mathcal{H}(0))^2 \rangle_m = \langle \dot{\Phi}^2 \int_0^t I(t') dt' \int_0^t I(t'') dt'' \rangle \\ &= \dot{\Phi}^2 \int_0^t dt' \int_0^t dt'' \langle I(t) I(t'') \rangle_m = \dot{\Phi}^2 \int_0^t dt' \int_0^t C(t', t''), \end{aligned} \quad (\text{B.4})$$

where  $C(t', t'') = \langle I(t) I(t'') \rangle_m$  is the current correlation function. If we further assume that  $C$  depends only on the difference between  $t'$  and  $t''$ , we can define  $\tau = t' - t''$ , and rewrite the energy dispersion as

$$(\Delta E)^2 = \dot{\Phi}^2 \int_0^t dt'' \int_{-t}^t d\tau C(\tau) = \left( \int_{-t}^t d\tau C(\tau) \right) \dot{\Phi}^2 t. \quad (\text{B.5})$$

Say  $(\Delta E)^2$  is dispersing, and if we use the relation  $(\Delta E)^2 = 2D_E t$  where  $D_E$  is the diffusion coefficient, we obtain

$$D_E = \frac{1}{2} \dot{\Phi}^2 \int_{-t}^t d\tau C(\tau). \quad (\text{B.6})$$

$\tilde{C}(\omega)$  is defined as the Fourier transform of  $C(\tau)$ ,

$$\tilde{C}(\omega) = \int_{-\infty}^{+\infty} e^{i\omega\tau} C(\tau) d\tau. \quad (\text{B.7})$$

At the DC limit,  $\omega \rightarrow 0$ , so we obtain

$$\tilde{C}(0) = \int_{-\infty}^{+\infty} C(\tau) d\tau. \quad (\text{B.8})$$

The diffusion approximation applies in the limit  $t \rightarrow \infty$ , and so we can write the diffusion coefficient as

$$D_E = \frac{1}{2} \tilde{C}(0) \dot{\Phi}^2. \quad (\text{B.9})$$

## Appendix C

# Connection Between Dissipation-Diffusion Relation and Kubo-Greenwood Formula

We will define  $C_m(t)$  as the current correlator that corresponds to an eigenstate  $|m\rangle$  of the Hamiltonian and can be written in bra-ket notation as

$$C_m(t) = \langle m | I(t) I(0) | m \rangle. \quad (\text{C.1})$$

Above  $I(t)$  has to be understood as the Heisenberg picture of the current operator i.e.  $I(t) = U^\dagger I_0 U$  where  $I_0$  is the time-independent current and  $U = e^{-i\mathcal{H}t/\hbar}$  is the time dependent evolution operator. We can then write

$$\begin{aligned} C_m(t) &= \langle m | U^\dagger I_0 U I_0 | m \rangle = \sum_n \langle m | U^\dagger I_0 | n \rangle \langle n | U I_0 | m \rangle \\ &= \sum_n \exp(iE_m t/\hbar) \langle m | I_0 | n \rangle \exp(-iE_n t/\hbar) \langle n | I_0 | m \rangle \\ &= \sum_n \exp(-i\omega_{nm} t) |\langle m | I_0 | n \rangle|^2, \end{aligned} \quad (\text{C.2})$$

if we define  $\hbar\omega_{nm} = E_n - E_m$ .

We will define  $C(t)$  as the current correlator, averaged over multiple nearby eigenstates is

$$C(t) = \langle C_m(t) \rangle_m = \frac{1}{M} \sum_{m,n} \exp(-i\omega_{nm}t) |\langle m|I_0|n \rangle|^2. \quad (\text{C.3})$$

The averaging over multiple states is essentially the same as averaging over micro-canonical ensembles used in the derivation. We will then take the Fourier transform of  $C(t)$ ,

$$\begin{aligned} \tilde{C}(\omega) &= \int dt C(t) \exp(i\omega t) \\ &= \int dt \frac{1}{M} \left( \sum_{m,n} \exp(-i\omega_{nm}t) |\langle m|I_0|n \rangle|^2 \right) \exp(i\omega t) \\ &= \frac{1}{M} \sum_{m,n} |\langle m|I_0|n \rangle|^2 \int dt \exp(i(\omega - \omega_{nm})t) \\ &= \frac{1}{M} \sum_{m,n} |\langle m|I_0|n \rangle|^2 2\pi \delta(\omega - \omega_{nm}). \end{aligned} \quad (\text{C.4})$$

If we consider that  $I_0 = ev/L$ , then  $\tilde{C}(\omega)$  can be written as

$$\tilde{C}(\omega) = 2\pi \left( \frac{e}{L} \right)^2 \frac{1}{M} \sum_{m,n} |\langle m|v|n \rangle|^2 \delta(\omega - \omega_{nm}). \quad (\text{C.5})$$

By applying this result to the Dissipation-Diffusion Relation version of the conductance of 3.3, we obtain the conductance form that is similar to the Kubo-Greenwood version of conductance of Section 3.2.

## Appendix D

# Hamiltonian in Adiabatic Basis

In the adiabatic basis, the basis vectors are the instantaneous eigenvectors of the Hamiltonian  $\mathcal{H}$ . We consider a Hamiltonian matrix of the form  $\mathcal{H} = \mathcal{H}_0 + \Phi I$ , where  $\mathcal{H}_0$  is the unperturbed Hamiltonian matrix,  $I$  the perturbation matrix, and  $\Phi$  the (scalar) perturbation strength. For a basis vector  $|n(\Phi)\rangle$ , we can find the corresponding energy eigenvalue using

$$\mathcal{H}(\Phi)|n(\Phi)\rangle = E_n(\Phi)|n(\Phi)\rangle. \quad (\text{D.1})$$

A vector  $|\psi\rangle = \sum a_n |n(\Phi)\rangle$  (where  $a_n = \langle n(\Phi)|\psi\rangle$ ) follows the time-dependent Schrödinger equation

$$\mathcal{H}\psi = i\hbar \frac{d\psi}{dt}. \quad (\text{D.2})$$

Using the definition of  $a_n$ , we can write

$$\begin{aligned} \frac{da_l}{dt} &= \left\langle l \left| \frac{\partial \psi}{\partial t} \right\rangle + \dot{\Phi} \left\langle \frac{\partial l}{\partial \Phi} \middle| \psi \right\rangle \\ &= -\frac{i}{\hbar} \langle l | \mathcal{H} \psi \rangle + \dot{\Phi} \sum_k \left\langle \frac{\partial l}{\partial \Phi} \middle| k \right\rangle \langle k | \psi \rangle \\ &= -\frac{i}{\hbar} E_l a_l + \dot{\Phi} \sum_k \left\langle \frac{\partial l}{\partial \Phi} \middle| k \right\rangle a_k. \end{aligned} \quad (\text{D.3})$$

To find the bracket term in the above equation, we will use the orthogonality condition  $\langle l(\Phi)|k(\Phi)\rangle = 0$  for  $l \neq k$ . If we take derivative of this with respect to  $\Phi$ , we obtain

$$\left\langle l \left| \frac{\partial k}{\partial \Phi} \right. \right\rangle = - \left\langle \frac{\partial l}{\partial \Phi} \left| k \right. \right\rangle. \quad (\text{D.4})$$

We will also use another orthogonality condition  $\langle l(\Phi)|\mathcal{H}(\Phi)|k(\Phi)\rangle = 0$  for  $l \neq k$ . Again, if we take the derivative of this equation with respect to  $\Phi$ , we get

$$\left\langle \frac{\partial l}{\partial \Phi} \left| \mathcal{H} \right| k \right\rangle + \left\langle l \left| \frac{\partial \mathcal{H}}{\partial \Phi} \right| k \right\rangle + \left\langle l \left| \mathcal{H} \right| \frac{\partial k}{\partial \Phi} \right\rangle = 0. \quad (\text{D.5})$$

From the Hamiltonian we see that  $\partial \mathcal{H} / \partial \Phi = I$ . Substituting Eq. D.5 to the above equation we obtain

$$\left\langle \frac{\partial l}{\partial \Phi} \left| k \right. \right\rangle = \frac{I_{lk}}{(E_l - E_k)}. \quad (\text{D.6})$$

Eq. D.3 can then be written as

$$\frac{da_l}{dt} = -\frac{i}{\hbar} E_l a_l + \dot{\Phi} \sum_{k \neq l} \frac{I_{lk}}{(E_l - E_k)} a_k. \quad (\text{D.7})$$

We will write  $\mathcal{H}(\Phi)|\psi\rangle$  in terms of the instantaneous basis vectors, and so we can assume that at an instant of time the basis vectors are constant, and hence

$$\begin{aligned} \mathcal{H}(\Phi)|\psi\rangle &= i\hbar \frac{d}{dt} \sum_l a_l |l\rangle = i\hbar \sum_l \frac{da_l}{dt} |l\rangle \\ &= \sum_l \left( E_l a_l + i\hbar \dot{\Phi} \sum_{k \neq l} \frac{I_{lk}}{(E_l - E_k)} a_k \right) |l\rangle. \end{aligned} \quad (\text{D.8})$$

If  $|\psi\rangle$  is one of the basis vectors, for example  $|m\rangle$ , the term for the coefficients are  $a_l = \delta_{lm}$  and Eq. D.8 can be written as

$$\begin{aligned} \mathcal{H}(\Phi)|m\rangle &= \sum_l \left( E_l \delta_{lm} + i\hbar \dot{\Phi} \sum_{k \neq l} \frac{I_{lk}}{(E_l - E_k)} \delta_{km} \right) |l\rangle \\ &= \sum_l \left( E_l \delta_{lm} + i\hbar \dot{\Phi} \frac{I_{lm}}{(E_l - E_m)} \right) |l\rangle \end{aligned} \quad (\text{D.9})$$

Hence we can write the matrix elements of  $\mathcal{H}$  in adiabatic basis representation to be

$$\begin{aligned}
\langle n|\mathcal{H}(\Phi)|m\rangle &= \langle n|\sum_l \left( E_l\delta_{lm} + i\hbar\dot{\Phi}\frac{I_{lm}}{(E_l - E_m)} \right) |l\rangle \\
&= \sum_l \left( E_l\delta_{lm} + i\hbar\dot{\Phi}\frac{I_{lm}}{(E_l - E_m)} \right) \delta_{ln} \\
&= E_n\delta_{nm} + i\hbar\dot{\Phi}\frac{I_{nm}}{(E_n - E_m)}
\end{aligned} \tag{D.10}$$

# Bibliography

- [1] C. W. J. Beenakker and H. van Houten, *Solid State Phys.* **44**, 1 (1991).
- [2] C. W. J. Beenakker, *Rev. Mod. Phys.* **69**, 731 (1997).
- [3] Y. Alhassid, *Rev. Mod. Phys.* **72**, 895 (2000).
- [4] B. Reulet, M. Ramin, H. Bouchiat, and D. Mailly, *Phys. Rev. Lett.* **75**, 124 (1995).
- [5] Y. Imry and N. S. Shiren, *Phys. Rev. B* **33**, 7992 (1986).
- [6] N. Trivedi and D. A. Browne, *Phys. Rev. B* **38**, 9581 (1988).
- [7] B. Reulet and H. Bouchiat, *Phys. Rev. B* **50**, 2259 (1994).
- [8] A. Kamenev, B. Reulet, H. Bouchiat, and Y. Gefen, *Europhys.* **28**, 391 (1994).
- [9] D. Cohen, T. Kottos, and H. Schanz, *J. Phys. A* **39**, 11755 (2006).
- [10] M. Wilkinson, B. Mehlig, and D. Cohen, *Europhys.* **75**, 709 (2006).
- [11] A. Miller and E. Abrahams, *Phys. Rev.* **120**, 745 (1960).
- [12] V. Ambegaokar, B. I. Halperin, and J. S. Langer, *Phys. Rev. B* **4**, 2612 (1971).
- [13] M. Pollak, *J. Non-Cryst. Solids* **11**, 1 (1972).
- [14] A. Stotland, R. P. Budoyo, T. Peer, D. Cohen, and T. Kottos, *arXiv:cond-mat/0712.0439*, 2007.

- 
- [15] A. Stotland, R. P. Budoyo, D. Cohen, and T. Kottos, in preparation, 2008.
- [16] J. Zhang, R. P. Budoyo, D. Cohen, and T. Kottos, work in progress, 2008.
- [17] P. W. Anderson, *Phys. Rev.* **109**, 1492 (1958).
- [18] B. Kramer and A. MacKinnon, *Rep. Prog. Phys.* **56**, 1469 (1993).
- [19] N. W. Ashcroft and N. D. Mermin, *Solid State Physics* (Brooks Cole, 1976).
- [20] E. N. Economou, *Green's Functions in Quantum Physics* (Springer, 1983).
- [21] D. J. Thouless, *J. Phys. C* **5**, 77 (1972).
- [22] M. Kappus and F. Wegner, *Zeitschrift für Physik B* **45**, 15 (1981).
- [23] D. J. Thouless, *Phys. Rev. Lett.* **39**, 1167 (1977).
- [24] E. Abrahams, P. W. Anderson, D. C. Licciardello, and T. V. Ramakrishnan, *Phys. Rev. Lett.* **42**, 673 (1979).
- [25] A. MacKinnon and B. Kramer, *Phys. Rev. Lett.* **47**, 1546 (1981).
- [26] D. Pines and P. Nozieres, *Theory of Quantum Liquids* (Westview Press, 1999).
- [27] C. Cohen-Tannoudji, B. Diu, and F. Laloë, *Quantum Mechanics* (Wiley-Interscience, 1977).
- [28] D. J. Griffiths, *Introduction to Quantum Mechanics* (Pearson Prentice Hall, 2004).
- [29] R. Kubo, *J. Phys. Soc. Japan* **12**, 570 (1957).
- [30] D. Greenwood, *Proc. Phys. Soc. London* **71**, 585 (1958).
- [31] J. T. Edwards and D. J. Thouless, *J. Phys. C* **5**, 807 (1972).
- [32] D. J. Thouless, *Phys. Rep.* **13**, 93 (1974).
- [33] E. N. Economou and C. M. Soukoulis, *Phys. Rev. Lett.* **46**, 618 (1981).
- [34] R. Landauer, *IBM J. Res. Dev.* **1**, 223 (1957).

- 
- [35] R. Landauer, *Philos. Mag.* **21**, 863 (1970).
- [36] E. N. Economou and C. M. Soukoulis, *Phys. Rev. Lett.* **47**, 973 (1981).
- [37] Y. Imry, *Introduction to Mesoscopic Physics* (Oxford University Press, 1997).
- [38] A. Kamenev and Y. Gefen, *Int. J. Mod. Phys. B* **9**, 751 (1995).
- [39] N. F. Mott, *Philos. Mag.* **22**, 7 (1970).
- [40] N. F. Mott and E. A. Davis, *Electronic processes in non-crystalline materials* (Clarendon Press, Oxford, 1971).
- [41] S. Bandopadhyay, Y. Etzioni, and D. Cohen, *Europhys.* **76**, 739 (2006).
- [42] A. Wobst, G. L. Ingold, P. Hänggi, and D. Weinmann, *Phys. Rev. B* **68**, 085103 (2003).
- [43] Y. V. Fyodorov, O. A. Chubykalo, F. M. Izrailev, and G. Casati, *Phys. Rev. Lett.* **76**, 1603 (1996).
- [44] A. Silva and V. E. Kravtsov, *Phys. Rev. B* **76**, 165303 (2007).
- [45] F. Foieri, L. Arrachea, and M. J. Sanchez, *Phys. Rev. Lett.* **99**, 266601 (2007).
- [46] A. D. Stone and A. Szafer, *IBM J. Res. Dev.* **32**, 384 (1988).
- [47] P. G. Harper, *Proc. Phys. Soc. London A* **68**, 874 (1955).
- [48] S. Aubry and G. André, *Ann. Israel Phys. Soc.* **3**, 133 (1980).
- [49] J. B. Sokoloff, *Phys. Rep.* **126**, 189 (1985).
- [50] G. L. Ingold, A. Wobst, C. Aulbach, and P. Hänggi, *Lect. Notes Phys.* **630**, 85 (2003).
- [51] K. Husimi, *Proc. Phys. Math. Soc. Japan* **22**, 264 (1940).
- [52] D. R. Hofstadter, *Phys. Rev. B* **14**, 2239 (1976).

- 
- [53] F. Borgonovi and I. Guarneri, *Phys. Rev. B* **52**, 3374 (1995).
- [54] R. Ketzmerick, K. Kruse, S. Kraut, and T. Geisel, *Phys. Rev. Lett.* **79**, 1959 (1997).
- [55] J. W. Brown and R. V. Churchill, *Complex Variables and Applications* (McGraw-Hill, 2003).
- [56] S. Weinberg, *The Quantum Theory of Fields* (Cambridge University Press, 1995).